NAVAL POSTGRADUATE SCHOOL

MONTEREY, CALIFORNIA

THESIS

AUTOMATED CONTROL OF A SOLAR MICROGRID–POWERED AIR COMPRESSOR FOR USE IN A SMALL-SCALE COMPRESSED AIR ENERGY STORAGE SYSTEM

by

Joshua N. Williams

June 2017

Thesis Advisor:	Anthony J. Gannon
Co-Advisor:	Andrea Holmes

Approved for public release. Distribution is unlimited.

THIS PAGE INTENTIONALLY LEFT BLANK

1. AGENCY USE ONLY *(Leave blank)*	2. REPORT DATE June 2017	3. REPORT TYPE AND DATES COVERED Master's thesis

4. TITLE AND SUBTITLE AUTOMATED CONTROL OF A SOLAR MICROGRID–POWERED AIR COMPRESSOR FOR USE IN A SMALL-SCALE COMPRESSED AIR ENERGY STORAGE SYSTEM	5. FUNDING NUMBERS
6. AUTHOR(S) Joshua N. Williams	

7. PERFORMING ORGANIZATION NAME(S) AND ADDRESS(ES) Naval Postgraduate School Monterey, CA 93943-5000	8. PERFORMING ORGANIZATION REPORT NUMBER
9. SPONSORING /MONITORING AGENCY NAME(S) AND ADDRESS(ES) Office of Naval Research with Technical Monitor of Marissa Brand and Richard Carlin	10. SPONSORING / MONITORING AGENCY REPORT NUMBER

11. SUPPLEMENTARY NOTES The views expressed in this thesis are those of the author and do not reflect the official policy or position of the Department of Defense or the U.S. Government. IRB number ____N/A____.

12a. DISTRIBUTION / AVAILABILITY STATEMENT Approved for public release. Distribution is unlimited.	12b. DISTRIBUTION CODE

13. ABSTRACT (maximum 200 words)

As part of the Office of Naval Research's study of advanced energy technologies, this research examined the development and implementation of a control system for the compression phase of a small-scale compressed air energy storage system, using a solar-powered microgrid to store energy as compressed air for later use. The compression system is composed of numerous commercial-off-the-shelf components wherever possible. All electronic components must also be able to communicate with the control system for proper operation. An industrial control system was selected for robustness, with an attached human-machine interface for system indications.

The compression system is powered by a solar microgrid that temporarily stores energy in ultracapacitors. This allows the compression system to run even when the available solar radiance is not sufficient to power the compressor directly. By monitoring the ultracapacitors and the available solar radiance, the control system can maximize the compressor run time during a given solar cycle, enabling the system to store the maximum amount of energy possible. This research demonstrates the use of a small-scale compressed air energy storage system as a viable long-term energy storage solution for microgrid applications.

14. SUBJECT TERMS compressed air, solar, energy storage, automation, industrial control	15. NUMBER OF PAGES 115
	16. PRICE CODE

17. SECURITY CLASSIFICATION OF REPORT Unclassified	18. SECURITY CLASSIFICATION OF THIS PAGE Unclassified	19. SECURITY CLASSIFICATION OF ABSTRACT Unclassified	20. LIMITATION OF ABSTRACT UU

i

THIS PAGE INTENTIONALLY LEFT BLANK

AUTOMATED CONTROL OF A SOLAR MICROGRID–POWERED AIR COMPRESSOR FOR USE IN A SMALL-SCALE COMPRESSED AIR ENERGY STORAGE SYSTEM

Joshua N. Williams
Lieutenant, United States Navy
B.S., University of South Carolina, 2010

Submitted in partial fulfillment of the
requirements for the degree of

MASTER OF SCIENCE IN MECHANICAL ENGINEERING

from the

NAVAL POSTGRADUATE SCHOOL
June 2017

Approved by: Anthony J. Gannon, Ph.D.
Thesis Advisor

Andrea Holmes
Co-Advisor

Garth V. Hobson, Ph.D.
Chair, Department of Mechanical and Aerospace Engineering

iii

THIS PAGE INTENTIONALLY LEFT BLANK

ABSTRACT

As part of the Office of Naval Research's study of advanced energy technologies, this research examined the development and implementation of a control system for the compression phase of a small-scale compressed air energy storage system, using a solar-powered microgrid to store energy as compressed air for later use. The compression system is composed of numerous commercial-off-the-shelf components wherever possible. All electronic components must also be able to communicate with the control system for proper operation. An industrial control system was selected for robustness, with an attached human-machine interface for system indications.

The compression system is powered by a solar microgrid that temporarily stores energy in ultracapacitors. This allows the compression system to run even when the available solar radiance is not sufficient to power the compressor directly. By monitoring the ultracapacitors and the available solar radiance, the control system can maximize the compressor run time during a given solar cycle, enabling the system to store the maximum amount of energy possible. This research demonstrates the use of a small-scale compressed air energy storage system as a viable long-term energy storage solution for microgrid applications.

THIS PAGE INTENTIONALLY LEFT BLANK

TABLE OF CONTENTS

THIS PAGE INTENTIONALLY LEFT BLANK

LIST OF FIGURES

LIST OF TABLES

LIST OF ACRONYMS AND ABBREVIATIONS

AA-CAES	Advanced Adiabatic Compressed Air Energy Storage
AC	Alternating Current
CAES	Compressed Air Energy Storage
CCW	Connected Components Workbench
DC	Direct Current
DOD	Department of Defense
DON	Department of the Navy
ESTEP	Energy Systems Technology and Evaluation Program
FBD	Function Block Diagram
HMI	Human Machine Interface
IMPEL	Integrated Multi-physics Energy Lab
J	Joules
kWh	Kilowatt-hour
MPPT	Maximum Power Point Tracking
NPS	Naval Postgraduate School
ONR	Office of Naval Research
PLC	Programmable Logic Controller
PSS-CAES	Polygeneration Small Scale Compressed Air Energy Storage
PV	Photovoltaic
SS-CAES	Small Scale Compressed Air Energy Storage
TCP/IP	Transmission Control Protocol/Internet Protocol
USNO	United States Naval Observatory
VAC	Volts Alternating Current
VDC	Volts Direct Current
Wh	Watt-hour

THIS PAGE INTENTIONALLY LEFT BLANK

ACKNOWLEDGMENTS

I would like to thank my advisors, Dr. Gannon and Andrea Holmes, for providing the opportunity to work on this project as well as extensive technical assistance with the solar-powered microgrid. Lastly, but most importantly, I would like to thank my wonderful wife, Ashley, for her tremendous support during this process.

THIS PAGE INTENTIONALLY LEFT BLANK

I.   INTRODUCTION

Energy is the foundation upon which our modern society is built. Without vast energy production capability, most modern amenities, which consume this energy, would become obsolete. In 2015, the United States consumed 28.529 trillion kilowatt-hours (kWh) (97.344 quadrillion BTU) of energy [1]. While over 80% of the energy consumed was fossil fuels, this accounts for fossil fuels used to produce electricity as well as other energy consumption means, such as automobiles and industrial processes. Fossil fuels accounted for 66.9% of the national electricity production during 2015 [1]. There has been a marked increase in greenhouse gasses over the past 165 years, as seen in Figure 1. As pointed out by the American Geophysical Union, "Fossil fuel burning dominates this increase. Human-caused increases in greenhouse gases are responsible for most of the observed global average surface warming of roughly 0.8°C (1.5°F) over the past 140 years" [2].
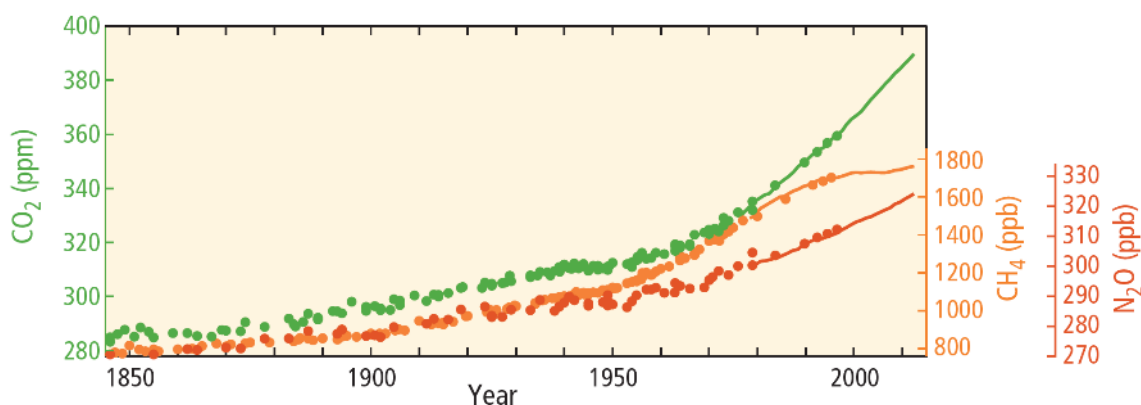
Figure 1.   Globally Averaged Greenhouse Gas Concentrations. Source: [3].

The U.S. Department of Defense (DOD) is certainly a culprit in this matter. During 2015, the U.S. Department of Defense consumed 215.4 million kWh (735.1 trillion BTU) of energy [1]. The majority of the DOD's energy expenditure during 2015 was in the form of fossil fuels for ships, tanks, and aircraft; however, there was still a significant consumption of fossil fuel by means of electrical energy at DOD installations.

DOD installations consumed 29.37 billion kWh of electricity during 2015, at a cost of $2.59 billion [4]. The Office of Naval Research (ONR) created the Energy Systems Technology and Evaluation Program (ESTEP) in fiscal year 2013 to promote the study of advanced energy technologies in real-world military installation settings [5]. ESTEP was created, through partnerships with educational institutions and industry, to develop and test advanced energy technologies that can be deployed to existing installations to reduce the financial burden of electricity consumption. The main objectives of the ESTEP program are [6]:

- Reduce costs

- Increase energy security

- Increase the reach and persistence of the warfighter

Recently, military commanders renewed their commitment to "forge ahead … with a decade-long effort to convert [their] fuel-hungry operations to renewable power" [7]. To put it succinctly, renewable energy is the future, and the impact that clean, renewable energy can have on our future as a nation and, ultimately, as a planet is unquestionable. The Sierra Club recently reported that "Nationally, clean energy jobs outnumber all fossil fuel jobs by over 2.5 to 1," which is a clear indicator of the trend toward clean energy production [8]. The renewable energy sector is constantly pushing the boundaries of innovation and production capacity, with "record-breaking generation" the new norm [9]. The portion of global energy produced from renewable sources continues to grow, with renewable sources accounting for more than half of the new production methods for the past two years, as seen in Figure 2 [10]. "Last year brought a hectic series of milestones for declining costs," further driving the market toward renewable energy [10].
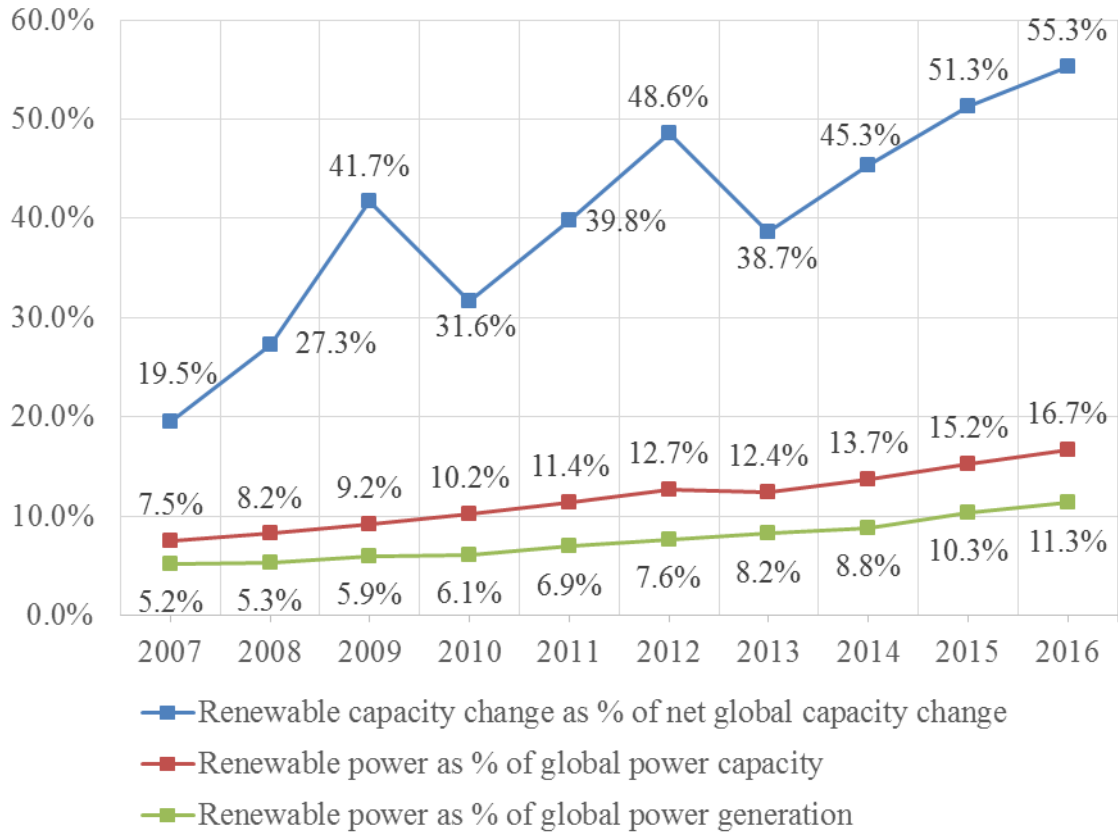
Figure 2.   Renewable Power Generation and Capacity as a Share of Global Power from 2007–2016. Adapted from [10].

For years, the cost of renewable power generation has dropped. The levelized cost of electricity (LCOE) is a method of comparing electricity production costs from various sources. By incorporating capital costs, maintenance costs, and fuel costs, the LCOE allows for comparison between a fossil fuel driven plant and a solar plant. From 2010 to 2015, the LCOE from on-shore wind generation dropped by 66% [11]. During the same 7-year period, the LCOE for photovoltaic (PV) solar generation dropped over 85% [11]. While this drastic drop in renewable energy cost has increased the availability of renewable energy sources on the grid, but this availability has created power quality issues due to the variable nature of renewable power generation.

As the renewable power generation market continues to grow, so too must the energy storage market to ensure continuous availability of clean power [12]. Peak

production, from solar specifically, has led to a glut of power due to the "high costs of restarting" conventional plants [13]. The grid currently relies on a costly system to minimize grid fluctuations, whereby some power plants remain in a "standby" state, ready to act as a "supplemental balancing reserve" [14]. This generally occurs since most renewable power sources produce outputs that vary according to numerous environmental factors. Wind power, for example, can be highly irregular and wind forecasting cannot completely mitigate this issue due to prediction errors [15]. When using PV cells, electricity production occurs as long as the sun is shining on the solar panels, which generally occurs during most daylight hours. If non-constant renewable power sources like wind and solar are to be used for major electricity production needs, there has to be a way to mitigate the variability in production capability [16]. Lazard projects that the levelized cost of energy storage will, over the next several years, incur a cost decline similar to the LCOE from renewable power generation [17].

A.   OBJECTIVES

The Naval Postgraduate School (NPS) Integrated Multi-Physics Energy Lab (IMPEL) houses several past, present, and future projects to study advanced energy production and storage systems in order to meet the future energy needs of the DOD. Some of these systems require automation to function properly, specifically, an off-grid solar powered microgrid and Small-Scale Compressed Air Energy Storage (SS-CAES) system. This thesis examines the development of an automated control system that stores energy as compressed air when the renewable energy produced by a solar microgrid exceeds the compressor power requirements. This energy can be stored indefinitely, until converted back to electricity through an expansion process. The expansion process is being similarly automated through work by Vranas [18].

B.   LITERATURE REVIEW

The most logical method for mitigating variable generation from renewable sources is to capture the excess energy during peak production times. Several studies have similarly concluded that power storage technologies are required to maintain stable power output from renewable sources [12, 19–22]. The energy storage technologies that

4

have been researched or implemented fall into three broad categories, as outlined in Table 1.

Table 1   Classes of Energy Storage. Adapted from [19].

Common Name	Required Discharge Time
Power Quality (Immediately availability)	Seconds to Minutes
Bridging Power (Short-term availability)	Minutes to 1 hour
Energy Management (Long-term availability)	Hours

Since the focus of this thesis is the automated control of an Energy Management system, further discussion of these technologies is in order.

1. Operating Utility-Scale Energy Storage

While numerous energy storage technologies have been researched and demonstrated, there are only two energy storage methods capable of long-term availability that are in operation on a utility scale [23]. The most widely used and most mature technology is pumped hydraulic storage (PHS) [16]. Globally, PHS can store over 90 GW of energy [24]. Pumped hydraulic storage uses an elevation offset of two reservoirs for energy storage. During non-peak electricity consumption hours, pumps use excess energy to move water from the lower reservoir to the higher reservoir. When demand peaks or variable production drops, water flows from the elevated reservoir through hydroelectric generators to produce electricity. One major advantage to PHS is that it is capable of storing vast quantities of energy. As noted by the U.S. Department of Energy, "a reservoir one kilometer in diameter, 25 meters deep, and having an average head of 200 meters would hold enough water to generate 10,000 MWh" [16]. Unfortunately, pumped hydraulic storage requires very restricting geographic features. Specifically, it requires a large change in elevation with the capability of storing vast quantities of water at both the high and low elevations.

Compressed Air Energy Storage (CAES) is the next most widely used long-term energy storage technology. A typical commercial CAES system is actually a hybrid storage technology, meaning it required additional heat input to generate power. There are only two commercial CAES plants in operation worldwide to date. They are located in Huntorf, Germany and McIntosh, United States [24]. These two commercial plants combined are capable of producing 400 MW from their stored air in conjunction with gas turbines [12]. The use of fossil fuels for heat addition actually classifies CAES as a "hybrid" energy storage system, since it relies on combustion as a heat source to expand the compressed air prior to entry into the power turbines. Figure 3 shows the schematic of a "hybrid" CAES facility.
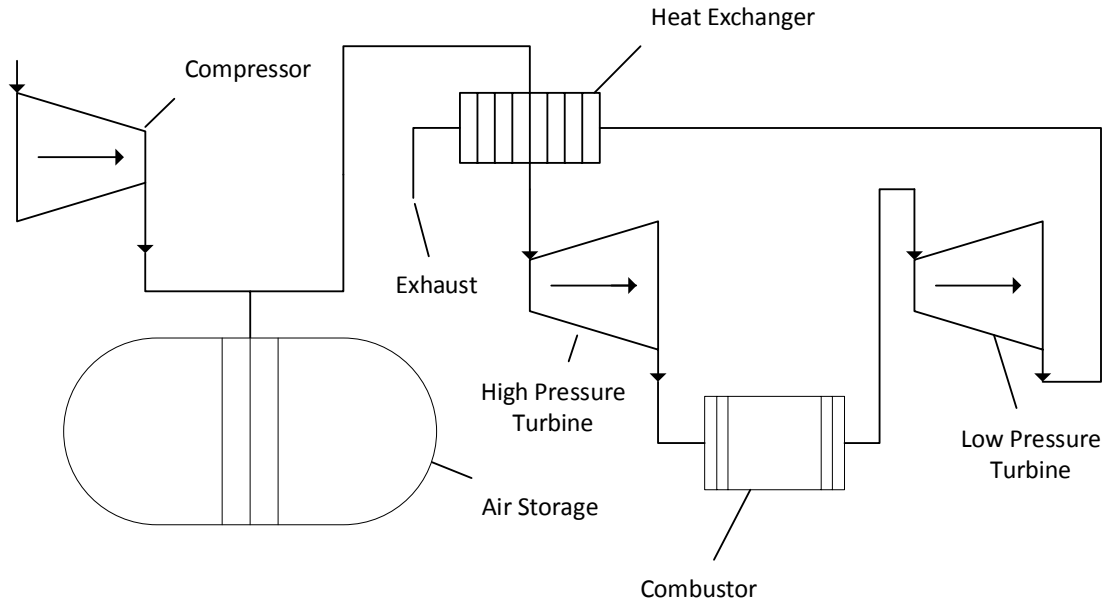
Figure 3.   General Hybrid CAES System Components. Adapted from [25].

Both commercial CAES plants in operation today have three significant drawbacks. First, these CAES plants use fossil fuels, which, as previously discussed, is not desirable due to the detrimental effects on the environment. While some of these effects can be reduced, there is no truly "clean" way to burn fossil fuels [26]. The second

6

drawback is that a single electrical motor/generator set couples to either the compressor or the turbines through clutching, as shown in Figure 4.
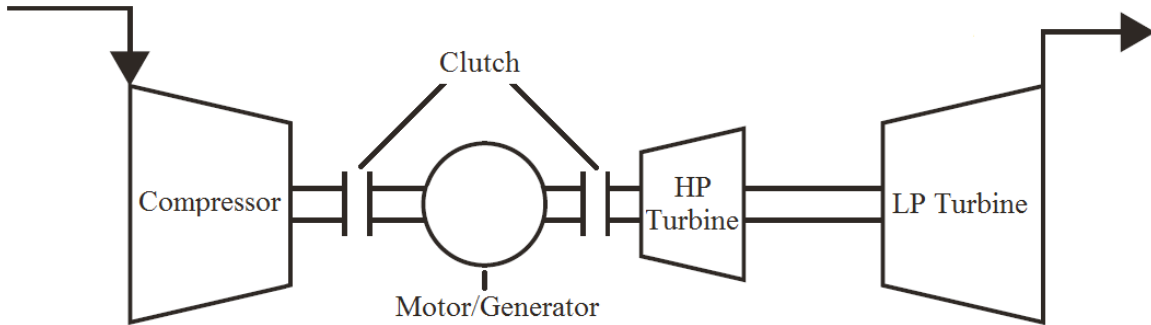
Figure 4. CAES Motor/Generator Clutch Arrangement. Adapted from [25].

Switching system alignment is not a quick process, as it requires physically decoupling the motor/generator set from one end prior to coupling it with the other, thus limiting a plant's response-time to energy demand changes [25]. Specifically, if immediate or short-term overproduction occurs with the CAES plant not aligned to compress air, the CAES plant cannot store the overproduction. Instead, conventional power plants must reduce production to meet demand, likely resulting in reduced plant operating efficiencies [27]. Lastly, commercial CAES plants use underground storage in salt caverns. While these salt caverns are more common than originally thought, this is still a geographic constraint and not feasible in many locations [24].

2. Conceptual Utility-Scale CAES Systems

Several utility scale CAES plants have been proposed over the past couple decades within the United States alone. These range from 200MW to 2700 MW in energy storage capability [28]. Unfortunately, indefinite postponement and abandonment are common among these CAES projects. As an example, the project to convert a former limestone mine in Ohio into a 2700 MW CAES facility was postponed due to "current market conditions, including low power prices and insufficient demand" [29]. A 270 MW CAES facility in Iowa that was planning to use an aquifer for storage was abandoned because all of the viable sites are "being used by the natural gas industry" for natural gas

storage [30]. As can be seen from just these two examples, the influx of cheap natural gas has threatened the advancement of CAES projects on multiple fronts [29, 30]. This implies that a cheaper type of CAES system with a different type of air storage system is required.

In 2002, the European Union commissioned a study titled Advanced Adiabatic – Compressed Air Energy Storage (AA-CAES) Project to develop a "zero CO2 emissions" CAES system [31]. An adiabatic CAES plant eliminates the largest drawback of traditional CAES plants: fossil fuel use. By examining Equation (1), we see that as air pressure rises during compression, air temperature will rise as well. Although Equation (1) is specific to ideal gases, it provides a simplified explanation of what happens to non-ideal gases undergoing compression [32].

$$T_2 = T_1 \left(\frac{P_2}{P_1} \right)^{(\gamma-1)/\gamma} \tag{1}$$

While a traditional CAES plant simply exchanges this heat with the surrounding environment, an adiabatic CAES system stores that thermal energy for subsequent use during expansion. Figure 5 shows a functional layout of this system. This not only eliminates the need to burn fossil fuels, it actually increases storage efficiency, resulting in a higher overall plant efficiency [31]. The AA-CAES Project examined both liquid and solid thermal energy storage (TES) media; unfortunately, neither type of TES medium is free of drawbacks. A liquid based TES system requires heat exchangers, pumps, and liquid storage tanks to ensure adequate heat transfer, complicating the overall design. A solid based TES system removes much of this added complexity, but requires pressure-rated TES housings as the compressed air interacts directly with the TES medium [31, 33].
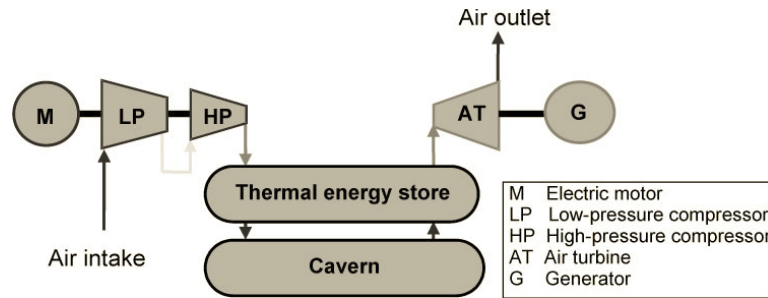
Figure 5. Function Diagram of an Adiabatic CAES Power Plant in Single-
Stage Configuration (Basic Layout). Source: [33].

RWE Power in Germany is developing an adiabatic CAES facility. The German project is named "Adiabate Druckluftspeicher für die Elektrizitätsversorgung" (ADELE), which translates to "adiabatic compressed-air energy storage (CAES) project for electricity supply" [34, 35]. Specifically, the use of the term adiabatic refers to the "additional use of the compression heat to increase efficiency," the system is certainly not free of heat transfer to the environment [35]. The ADELE project intends to use a specially designed tank filled with engineered TES stones arranged in a "packed bed" [36]. During compression, the hot compressed air passes through the tank, from top to bottom, transferring the heat to the engineered TES stones. Figure 6 shows this schematically for a two-stage system. Then, during expansion, the cool compressed air passes through the thermal storage tank again, this time from bottom to top, transferring the stored heat back to the air just prior to expansion. This greatly simplifies the TES system when compared to oil based thermal storage systems [31].
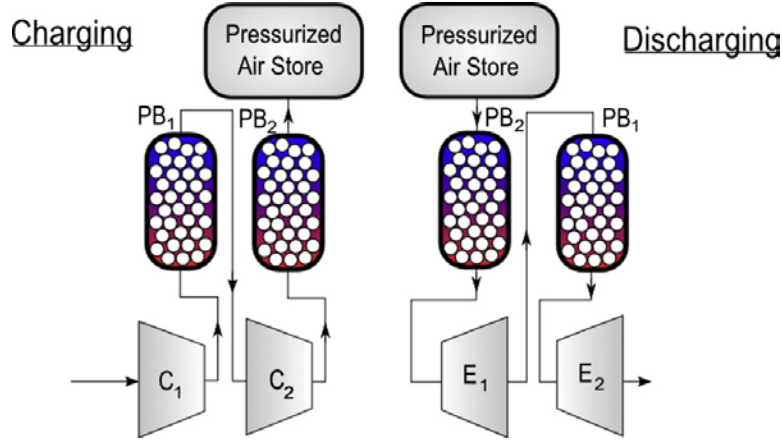
Figure 6.   Schematic of an Adiabatic CAES System with Packed Bed TES.
Source: [36].

3.   Small-Scale Energy Storage

A study in 2013 by Petrov et al. examined a distributed CAES system as a means of providing balancing power to the grid. The concept examined the use of multiple SS-CAES plants distributed across the grid at "residential homes" and "commercial buildings" to offset the variability in energy production inherent with wind and solar power [37]. In this study, the SS-CAES plants examined were purely adiabatic, meaning that there was no heat exchange occurring during or after compression. Instead, the proposed aboveground air storage tanks store the hot compressed air, maintaining its heat through use of insulating materials. While not as efficient at power conversion as battery storage, this approach yielded a theoretical energy storage efficiency of 75.2%, which is significantly higher than current CAES systems and "matches the efficiency of low-tech battery systems" [25, 37]. Even taking into account potential real-world losses, the efficiency of this system at least matches currently available CAES systems. This increased efficiency, paired with the significant cost advantage of SS-CAES over comparably-sized battery storage, looks rather promising for grid energy storage [37].

In 2014 Jannelli, et al. examined the use of an adiabatic SS-CAES for powering a remote radio communications tower in Italy. In addition to providing the electrical power for the communications tower, the authors examined the use of the cool turbine exhaust to cool sensitive electronic equipment. The resulting cycle was termed a Polygeneration

SS-CAES (PSS-CAES) due to the multiple methods of energy output. The proposed PSS-CAES system stores the heat of compression in a TES oil, allowing more air mass storage per unit volume when compared to the system devised by Petrov, et al. [37, 38]. Although this PSS-CAES system uses a more complex TES oil system, the ability to compress the air in stages and remove the heat of compression produces a more efficient system overall [38].

At Clemson University, Patel, et al. demonstrated a Hybrid SS-CAES system in 2014. The study centered on a solar microgrid to compress air and a small propane powered turbine. Figure 7 shows the power flow for this Hybrid SS-CAES system. Although this system uses fossil fuels, Patel, et al. were able to increase electricity production by 69.3% while burning the same amount of fuel. The solar powered air compression system led to this accomplishment, and ultimately achieved an overall system efficiency gain of 8.1% [39]. While this study included the use of fossil fuels, the increase in overall system efficiency reduces the "carbon footprint" of this microgrid, making it more environmentally friendly [39].
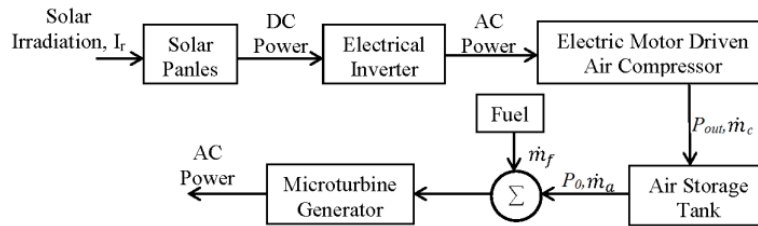
Figure 7.   Power Flow Diagram for Electrical Microgrid. Source: [39].

The year 2016 saw multiple renewable energy storage projects at NPS IMPEL as well. In June 2016, Hawxhurst developed and implemented a thermal storage control system for an off-grid wind and solar-powered microgrid. This project automatically matched the thermal storage capability to the available power. Storing power as thermal energy demonstrates a direct end-use case for heating and cooling applications [40]. By December 2016, McLaughlin demonstrated a means of generating power from compressed air using commercial off-the-shelf technology [41]. Also in December 2016,

Prinsen designed, and performed thermodynamic analysis of the NPS IMPEL SS-CAES plant [42]. This thesis further examines the implementation of the system designed by Prinsen, and the automation thereof.

II.   EQUIPMENT AND COMMUNICATIONS

The development of the SS-CAES system at NPS IMPEL is propagating along two separate, but related paths. McLaughlin initially implemented the power generation or expansion phase with further automation by Vranas [18, 41]. Prinsen examined the overall theoretical SS-CAES system performance and selected the exact components required for the compression system based on the already available air storage tanks [42]. Figure 8 shows a simplified diagram of the energy flow for the supply side of the solar-powered SS-CAES system at NPS IMPEL. This thesis continues with the supply side, or compression phase development.
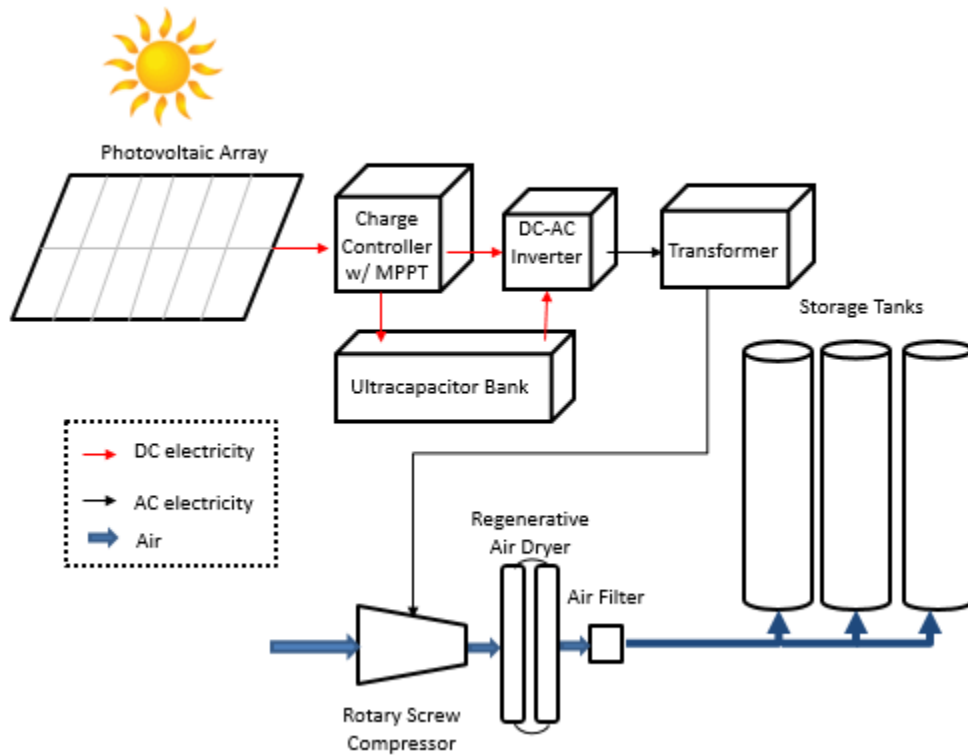
Figure 8.   Simplified Diagram for Supply Side of Solar-Powered, SS-CAES.
Source: [42].

A. EQUIPMENT

The various mechanical and electrical devices that facilitate the capture, conversion, and storage of energy for the solar-powered SS-CAES are described herein.

1. Electricity Production

The PV array that constitutes the source of electricity for this project is comprised of 12 panels, each rated at 280 watts of peak power, for a maximum power generation of 3.36kW. The array covers an area of 19.3 m^2 (207.7 ft^2) and is arranged in six parallel strands, each with two panels in series, to provide a maximum of 79 Volts Direct Current (VDC) to the charge controller [43]. Figure 9 shows the PV array used for the NPS IMPEL SS-CAES system.
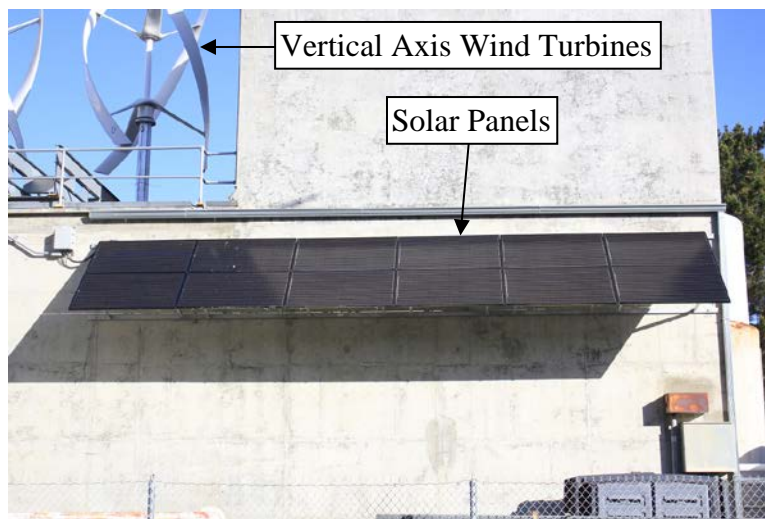
Figure 9.   SS-CAES PV Array at NPS IMPEL

2. Charge Controller

The power produced by the PV array is supplied to a MidNite Solar Classic 150 charge controller. The Classic 150, shown in Figure 10, is a Maximum Power Point Tracking (MPPT) charge controller. An MPPT controller continuously samples the available voltage and current from both the PV array and the storage medium. It then determines the optimum voltage and current to output to the storage medium in order to achieve maximum power transfer from the PV array to the storage medium. Using an MPPT controller provides the maximum power possible to the storage medium, which greatly increases the power availability and efficiency of the entire microgrid system [44]. Figure 11 illustrates the further power extraction capable with an MPPT type charge controller. Additionally, the Classic 150 supports Modbus protocol via TCP/IP for communication.

Figure 10.   MidNite Classic 150 Charge Controller and E-Panel
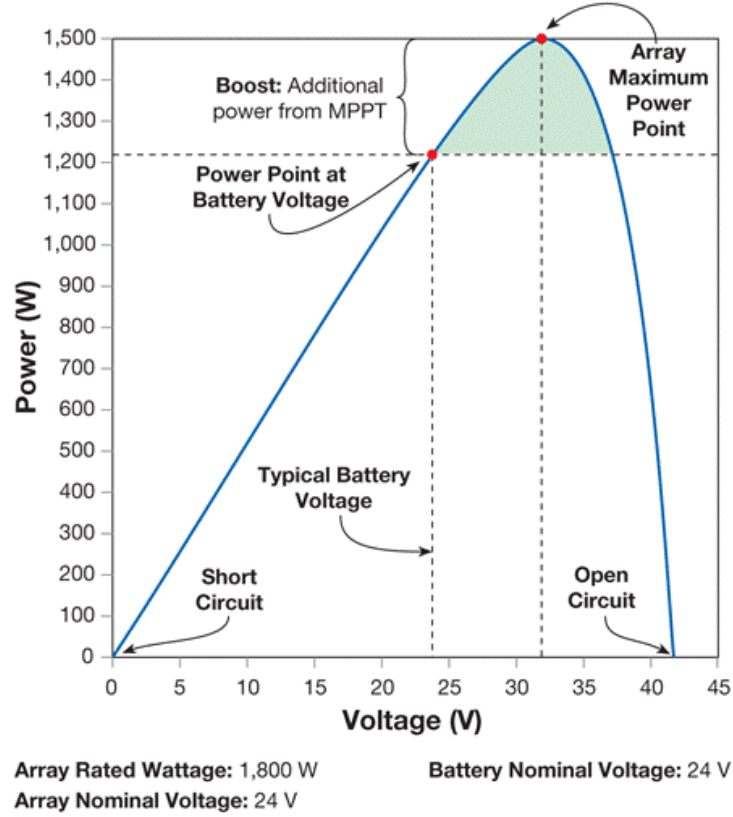
Figure 11.   Typical Maximum Power Point Tracking Controller Advantage.
Adapted from [45].

3.   Temporary Energy Storage Medium

The temporary energy storage medium for the solar microgrid is composed of an array of ultracapacitors. Six Maxwell BMOD0130 P056 B03 ultracapacitors, shown in Figure 12, rated at 56 VDC arranged in parallel provide a total of 780 farads of capacitance. The total energy stored in the capacitor bank in watt-hours (Wh) can be obtained from Equation (5), which is derived from a combination of Equations (2) through (4) [46].

$$C = \frac{Q}{V} \tag{2}$$

C is capacitance in farads. Q is the charge on the capacitor at full voltage in coulombs. V is the voltage.

$$E = \frac{1}{2}\frac{Q^2}{C} \qquad (3)$$

E is energy stored in the capacitor in joules (J). Q and C are as in Equation (2).

$$E = \frac{1}{2}CV^2 \qquad (4)$$

Finally, Equation (5) converts the energy in J to the more useful Wh units.

$$E[Wh] = E[J]\left(W\frac{s}{J}\right)\left(\frac{h}{3600s}\right) \qquad (5)$$

It is important to note that the capacitors only charge to 54.5 VDC to prevent exceeding their rated voltage. While this prevents damage to the capacitors through the process of dielectric breakdown, it also reduces the total energy storage possible. Based on the maximum charged voltage of the capacitor bank, 321.8 Wh are available for energy storage.

Figure 12.   Maxwell BMOD0130 P056 B03 Ultracapacitor. Source: [47].

4. DC to AC Inversion

An SMA Sunny Island 4585-US-10 inverter, shown in Figure 13, produces a single 120 volts alternating current (VAC) phase. This 120 VAC feeds into an SMA SI-TD-BOX-10 Smartformer to transform the 120 VAC to a 240 VAC supply, which ultimately powers the compressor and air dryer.

Figure 13.   Sunny Island 4585-US-10 Inverter

5. Inverter Monitoring

A critical component for monitoring the PV plant is the SMA Sunny WebBox, shown in Figure 14. This device provides Modbus support for the connected SMA Sunny Island inverter via Ethernet cable. Since the Sunny Island inverter does not support the Modbus protocol, the WebBox acts as a communication interface to allow communication with the controller. Additionally, the WebBox provides a means of monitoring and modifying SMA equipment parameters through a web-based interface that can be accessed via computer. The WebBox required both a firmware update and a device profile update to support Modbus communication, the details of which are contained in Appendix F.
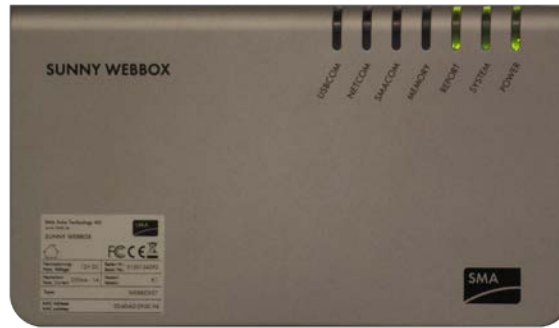
Figure 14.   SMA Sunny WebBox

6.   Air Compressor

The compressor installed for the SS-CAES system is a Powerex SF020872AJ. This compressor, shown in Figure 15, is rated at 1.5 kW (2 HP) and is capable of producing $0.17m^3$ (6 ft^3) of air at 689.5 kPa (100 psi). An oil-less scroll compressor was selected due to its minimal maintenance requirements and a continuous duty cycle, allowing for long run periods with minimal downtime for maintenance. If the compressor has power, it will automatically cycle on and off at 655 kPa (95 psi) and 792.9 kPa (115 psi) respectively based on an internal pressure switch.

Figure 15.   Powerex Oil-less Scroll Air Compressor

7. Air Storage Tanks

The backbone of the SS-CAES system at NPS IMPEL is the air storage tanks. While there are four tanks shown in Figure 16, only three of them are in use. They are capable of holding approximately 133 m^3 (4697 ft^3) at 2068 kPa (300 psi) and initially supported just the operation of the supersonic wind tunnel at the NPS Turbomachinery Lab [42]. The calculations of tank volume and total stored energy for the SS-CAES system are in Appendix A. By approximating the expansion process as adiabatic, a relatively valid assumption, Equations (6) through (8) can be used to determine the total energy stored in these air tanks [32]. The main IMPEL compressor has the capability to compress air to 792.9 kPa (115 psi). Thus the installed air tanks were calculated to contain approximately 32.63 kWh of energy in the form of compressed air.

$$PV^\gamma = \text{constant} \tag{6}$$

$$V_2 = \left(\frac{P_1}{P_2}V_1^\gamma\right)^{1/\gamma} \tag{7}$$

$$_1W_2 = \int PdV = \frac{P_2V_2 - P_1V_1}{1-\gamma} \tag{8}$$

Figure 16.   Air Storage Tanks at NPS IMPEL

8.   Air Dryer

Additional considerations for humidity were necessary due to the required air quality for use during supersonic wind tunnel operations. This resulted in the need for an air dryer to be incorporated into this system. As this system is a proof-of-concept, these limitations, as well as the occasional use of the supersonic wind tunnel are simply accepted due to the significant investment what would be required to procure a complete set of air storage tanks. The air for the supersonic wind tunnel is required to be extremely dry, with a dew point below -40 °C. To achieve this, the air passes through a Parker K-MT2 non-heated regenerative desiccant type air dryer, shown in Figure 17. A non-heated regenerative desiccant type dryer was selected since it requires significantly less power to operate than a heated regenerative desiccant air dryer.

Figure 17.   Parker K-MT2 Air Dryer

9.   Plant Control System

The controller selected for automation was an Allen-Bradley Micro850 programmable logic controller (PLC). Additionally, an Allen-Bradley PanelView 800 Human Machine Interface (HMI) Terminal provides indication of the overall plant status and the ability to manually operate the equipment. The PLC and HMI are shown in Figure 18 and Figure 19, respectively. PLC type controllers have several advantages over personal computer (PC) based controllers, and these advantages are the main drive for the selection of a PLC type controller [48]. Ensuring that a power failure would not cause data corruption and ultimately render the entire system inoperable was the primary concern, and is something that occurs with traditional PC based control systems. An additional advantage of the Micro850 is that it provides direct relay control without any additional components, while still having several expansion ports to allow for added functionality if required. Both the compressor and air dryer receive power through Crydom CMRD4845 solid-state relays. The PLC provides the required signal to operate the relays, thereby providing power to both the compressor and air dryer. A solid-state relay requires significantly less power to operate than a comparably sized mechanical

22

relay, which provides further power savings [49]. The initial setup required to program the PLC and HMI are contained in Appendix B.

Figure 18.   Allen-Bradley Micro850 Controller

Figure 19.   Allen-Bradley PanelView 400 HMI

B.   SYSTEM AND EQUIPMENT LIMITATIONS

While the capacitor bank can store 321.8 Wh of energy, not all of that energy is usable with the installed components. It was discovered that the Sunny Island inverter requires at least 30 VDC at its input to operate and provide AC power. The 30 VDC low-voltage limit of the Sunny Island inverter prevents the use of any capacitor energy stored below 30 VDC. To prevent reaching this limit and causing faults on the inverter, 31 VDC is the lowest voltage allowed on the capacitors by the PLC during automatic operation.

By again using Equations (4) and (5), the total capacitor energy available for conversion to usable power is determined to be only 217.7 Wh, a reduction of 32.4%.

While this system is intended to be a stand-alone microgrid, the building power grid is capable of providing power to the compressor regardless of inverter status. Breakers turn this functionality on or off as desired. This allows unlimited testing of the compression system, regardless of the PV array output. However, this also presents an issue as there is a dropout relay that is controlled by the MidNite Classic 150 charge controller, which is in line with the compressor input. When capacitor voltage drops below a preset value, the system will automatically attempt to shift to grid power. If the grid breaker is off, the compressor will lose power when the low voltage dropout relay switches position, even though the inverter will continue to operate. Selecting "Relay On" for the MidNite Classic 150 Aux1 mode prevents automatic cycling; thus ensuring the solar microgrid and inverter continuously power the compressor. As added protection for the inverter, the set point for the dropout relay in the MidNite Classic 150 was set to 30.5 VDC to prevent inverter faults when the PLC is controlling the compressor via the manual operation mode.

Due to the numerous communications methods and update frequency of inverter parameters, which will be discussed further, there are some issues with receiving data in real-time. Specifically, the exact status of the inverter cannot be known with certainty for approximately 30 seconds after it is started or stopped. Since the controller must know the state of the inverter prior to starting the controller, a method had to be devised that would account for this delay. This method will be discussed further in the Methods & Testing chapter.

The last, and likely the greatest limitation, arises from the Sunny Island inverter. As previously discussed, the inverter itself will not operate at voltages below 30 VDC. Additionally, its charge controller is not compatible with charging capacitors. The Sunny Island inverter will place itself into a self-protect mode below approximately 25 VDC and power off, which requires a physical reset of the inverter of "at least 15 minutes before restarting the Sunny Island" [50]. The Sunny Island also draws significant power from the capacitors, even while in standby. This results in the Sunny Island inverter

draining the capacitor bank after sunset if the inverter is left on. Therefore, if the inverter breaker is not switched off at the end of each day, the inverter will enter self-protect mode, power off, and the control system will fail to operate as intended. Unfortunately, there is no simple way to bypass this limitation; however, this issue will be eliminated once the expansion and compression portions of the NPS IMPEL SS-CAES system are fully integrated.

C. METHODS OF COMMUNICATION

Numerous communications protocols allow communication between the electronic components of the power and control systems. Figure 20 shows a graphical representation of these communication protocols as they apply to the power and control system.

1. Multi-protocol Ethernet

The Allen-Bradley Micro850 controller uses an Ethernet cable to communicate via Transmission Control Protocol/Internet Protocol (TCP/IP). The Micro850 is able to communicate with multiple devices using supplementary protocols that rely on the TCP/IP structure for data transmission.

2. Allen-Bradley CIP via Ethernet

The Micro850 controller and the PanelView 800 HMI communicate with each other via an industrial network that uses "Control an Information Protocol" (CIP) over Ethernet, which transmits data between the devices using TCP/IP. While Allen-Bradley CIP via Ethernet was developed to "allow for plug-and-play among complex devices from multiple vendors," only Allen-Bradley controllers commonly use it due to strict licensing requirements [51].

Sunny Island Inverter

MidNite Classic 150

Ethernet Switch

Sunny WebBox

PanelView 800 HMI

Micro850 Controller

- Multi-protocol Ethernet
- Common Industrial Protocol
- Modbus via TCP/IP
- SMA Fieldbus
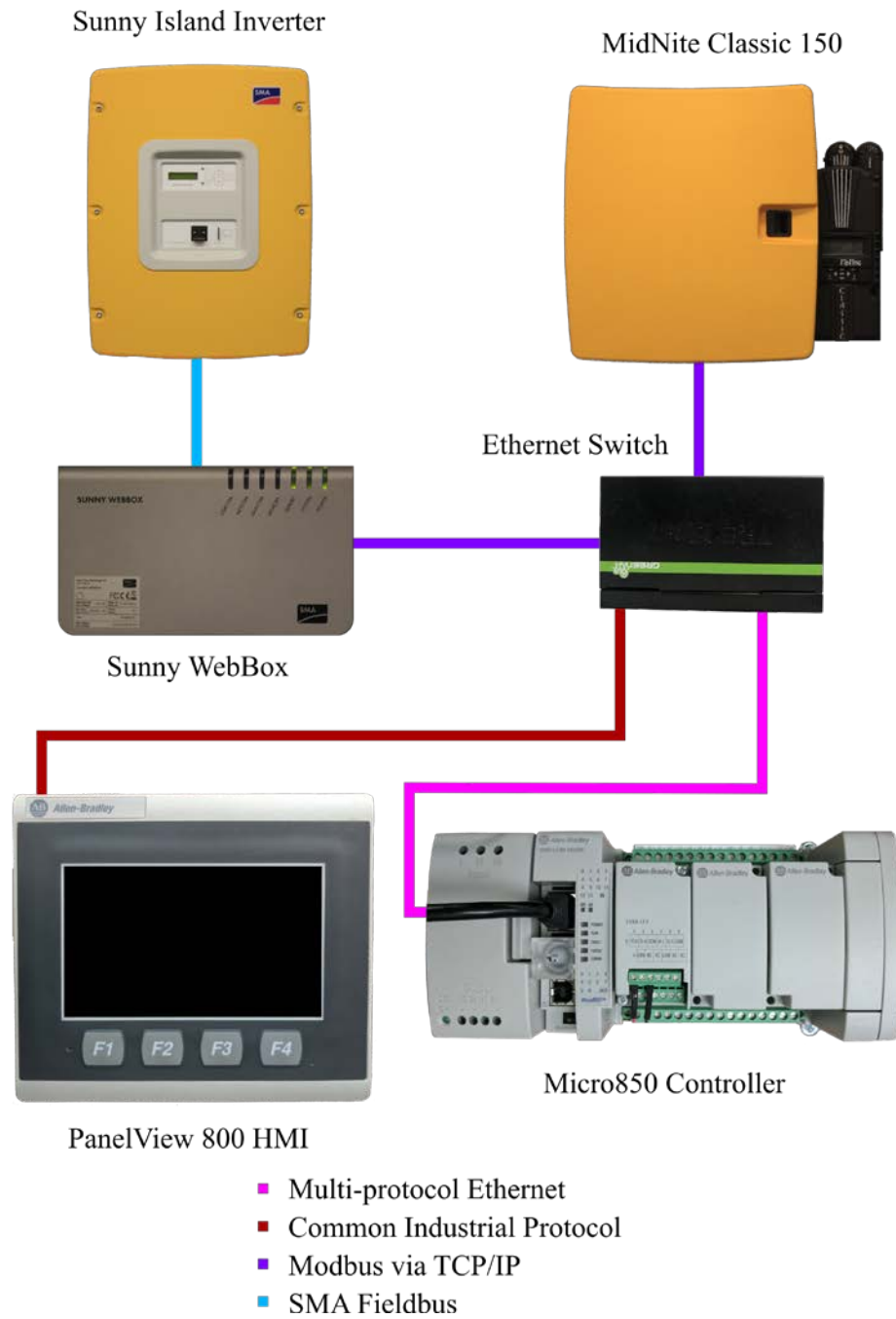
Figure 20.   Communications Map

3. Modbus via TCP/IP

The Modbus protocol allows for communications between the controller and both the Sunny WebBox and the MidNite Classic 150 charge controller. Modbus has been widely used throughout industry since its inception in 1978. Modbus makes communication between controllers and sensors in factories easy to implement. Its standardization ensures equipment from different manufacturers can communicate effectively. This allows for rapid deployment of large networks of connected devices. Modbus operates in a master/slave type system where one master controls all slaves [52]. The Modbus network created for this thesis is comprised of three devices, the Allen-Bradley Micro850 controller, the Sunny WebBox, and the MidNite Classic 150. The Micro850 controller serves as the network master, while the remaining two devices are slaves. The Sunny WebBox can only function as a slave and serves as a gateway to the devices attached to it [53]. Modbus is not enabled by default on the WebBox, and must be enabled via the web interface. Details for enabling Modbus on the WebBox are contained in Appendix F. Modbus is enabled by default on the MidNite Classic 150.

A separate program titled AssignID was written for the Allen-Bradley Micro850 and the Allen-Bradley PanelView 800 HMI Terminal to ensure that the correct Modbus addresses were being used, and verify Modbus parameters prior to implementation in the full-system control program. This was necessary to determine if the listed addresses for components were memory addresses or register locations. As noted by MidNite Solar:

> The Modbus specification adds one (1) to the "address" sent to the unit in the packet command to access a "register". This is so that Modbus registers start at 1 rather than 0. The main Classic address map starts at register 4101 but the packet itself sends out address 4100. Some Modbus software and libraries will go by register number and some will go by address so make sure which one it works with. [54]

This program allows the user to change in real-time the client being accessed, the Modbus register being accessed, the access mode, the expected command, and the command or response size. Additionally, it allows the user to see real-time data contained within the Modbus response, which allows the user to verify the correct Modbus address is in use. The details of this program are contained in Appendix E.

4.   SMA Fieldbus

The SMA Sunny Island inverter and the SMA Sunny WebBox communicate through a dedicated connection called the SMA fieldbus. This proprietary connection allows communication between SMA devices only. Only the WebBox is directly accessible via Modbus, but it does serve as a gateway for Modbus communication to other SMA connected equipment via the SMA fieldbus. The SMA fieldbus utilizes a master/slave type system similar to Modbus; however, it differs in that the WebBox is the master on the SMA fieldbus and the remaining SMA devices are slaves.

III. METHODS AND TESTING

This chapter covers the basic approach to the programming and testing of the control system for the compressor used in the CAES system at the NPS IMPEL.

A. CONTROL APPROACH

Since the added complexity of a variable speed drive would outweigh any real-world benefits for a system of this size, a single speed compressor was chosen [55]. This greatly simplifies the overall system design, and the coding required by restricting the compressor to be either running or secured. However, numerous real-world variables can only be determined in real-time for full automation. These variables include available sunlight for power generation, the status of the inverter, the voltage of the capacitor bank, and the desire for manual operation. Figure 21 shows the overall control program flowchart. The details of the PLC and the HMI programs are contained in Appendix C and Appendix D respectively.

1. Loss of Power Protection

One feature of the Micro850 is that it will retain global variables after power is lost and subsequently restored. Global variables are the only variables that can transmit between the Micro850 and the PanelView 800. This leads to a problem where several variables do not reset following a loss and subsequent restoration of power, which may lead to undesired equipment operation. Using the SYSVA_POWERUP_BIT, which is only TRUE during the first run through the code after power-up, any variables that may lead to undesired equipment operation are set to safe values prior to any other code execution, thus ensuring a safe power-on state [56].

2. Indication of Program Stall

Another issue that might arise is the stalling of either the Micro850 or the PanelView 800 HMI. To provide the user with indication that the system is operating as intended, a heartbeat indicator is present in the top right of the screen. By flashing on and off, this heartbeat indicator demonstrates that there is continuous communication between

the Micro850 and the PanelView 800 HMI and that no lock-up or stall has occurred on either device.
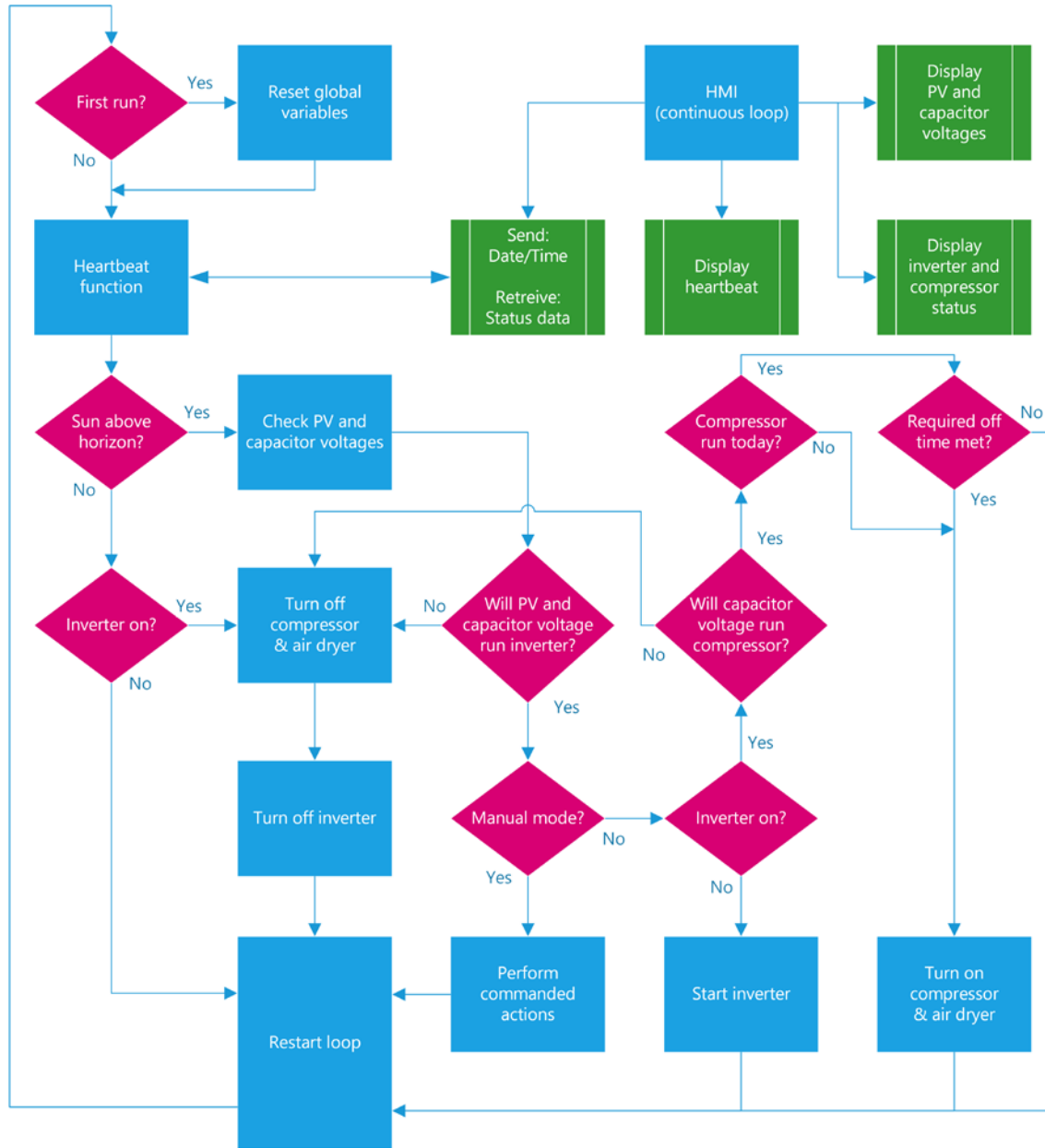
Figure 21.   Simplified Control Program Flowchart

3. Solar Power Production Status

Since the air compressor cannot function without sufficient solar power, it is imperative that proper tests are conducted to ensure sufficient power is available prior to and during operation of the compressor. A combination of three tests ensures that there is sufficient solar power available.

The first test performed checks the date and time against a stored value of sunrise and sunset times. The Micro850 does not contain a real-time clock; however, the PanelView HMI does contain a real-time clock, and is able to communicate the current date and time to the Micro850 for use during the following checks. The sunrise and sunset times were obtained from the United States Naval Observatory (USNO), and are specific to the location of the installed PV array at the Naval Postgraduate School Multi-Physics Renewable Energy Laboratory [57]. The most limiting sunrise and sunset times throughout the month were determined. These are the latest sunrise time and the earliest sunset time within the month. This resulted in 12 conservative sunrise and sunset times for use during the year. Using the limiting values ensures that the sun is at least above the horizon prior to commencing the second test.

The second test specifically looks at the voltage across the PV array. Verifying that the voltage across the PV array is at least 55 VDC ensures that sufficient power production exists to keep the capacitors above the 30 VDC cutoff voltage of the Sunny Island inverter. The cutoff voltage was determined by allowing the Sunny Island inverter to run continuously until it automatically shut off, which occurred at a capacitor voltage of 25 VDC, with the initial faults occurring at 30 VDC. To prevent any faults that might affect system operation, an operational limit of 31 VDC has been imposed. Verifying the PV array voltage directly allows the system to compensate for variable conditions such as cloud cover. To prevent rapid cycling of the system in the event of intermittent clouds, the system will not shut down the compressor or inverter until PV array voltage drops below 50 VDC. The upper PV array voltage limit is based on the minimum observed voltage capable of continuous compressor operation. The lower PV array voltage limit is based on the PV array producing enough power to maintain the capacitor bank voltage above the inverter shut-off limit of 30 VDC.

The last test performed verifies that sufficient power is available by directly measuring the capacitor voltage. The state of charge of the capacitor bank is determined directly through its voltage. The previous test examined the PV array voltage, which ultimately charges the capacitors; however, the state of charge of the capacitor bank is equally important. Verifying that the capacitor voltage is above 33 VDC prior to starting the compressor ensures that there is sufficient reserve power in the capacitors to continue inverter and compressor operation without fear of an automatic inverter shutdown. Again, to prevent rapid cycling, the compressor will not shut down until the capacitor voltage drops below 32 VDC.

4.   Inverter State

As previously discussed, the delay in real-time inverter status causes some issues. Specifically, the controller may attempt starting the compressor when no power is actually present. To eliminate this issue, an inverter-commanded-off bit is set indicating that the inverter is off after the shutdown command has been sent. A delay of 45 seconds is implemented to ensure the true status of the inverter is updated prior to resetting the inverter-commanded-off bit. This prevents the controller from attempting to start the compressor when no input power is available.

5.   Compressor Restart Delay

After the first time the compressor has run on a given day, a compressor-run-today bit is set. This bit in conjunction with a minimum-voltage-to-run set point, or shut-off set point, account for the possibility of the compressor drawing more power than is available. Should running the compressor lower the voltage of the capacitors to the shut-off set point, the compressor will be turned off to allow the capacitors to recharge. The capacitors must subsequently charge above a minimum-voltage-to-restart set point before the controller will restart the compressor. Additionally, a minimum charge time of ten minutes is enforced to ensure sufficient power is stored in the capacitors prior to restarting the compressor. The ten minute delay and minimum-voltage-to-restart set point combine to ensure the compressor has sufficient power for a substantial run prior to starting again.

6.   Manual Control Capability

The HMI provides users with an option to place the system into manual mode. While in manual mode, the system will not automatically start or stop the compressor or inverter. This mode provides the user a method for turning off the compressor and/or the inverter when they would normally be automatically controlled, to allow for system maintenance and troubleshooting. The manual mode will not allow the inverter to start without appropriate voltage on both the PV array and on the capacitors; however, there is no automatic off to prevent faults on the inverter. Additionally, while in manual mode, it is possible to start and stop the compressor from the grid with the inverter off. Continuous monitoring is required if the system is operated in this mode. Should the controller lose power while in manual mode, it will resume operation in manual mode upon power restoration; however, the compressor and inverter will not automatically restart if they were previously running.

7.   Other Considerations

The control system performs no direct pressure monitoring since the compressor will automatically turn on and off as previously discussed. As shown in Figure 22, the existing building arrangements dictated the location for installing the compression equipment. The significant distance between the power and control center and the compression equipment presented multiple obstacles to implementing direct pressure measurement. As such, the cycling of the compressor by pressure switch combined with the low power consumption of the solid-state relay present an adequate pressure control with minimal power requirements for this proof-of-concept system.
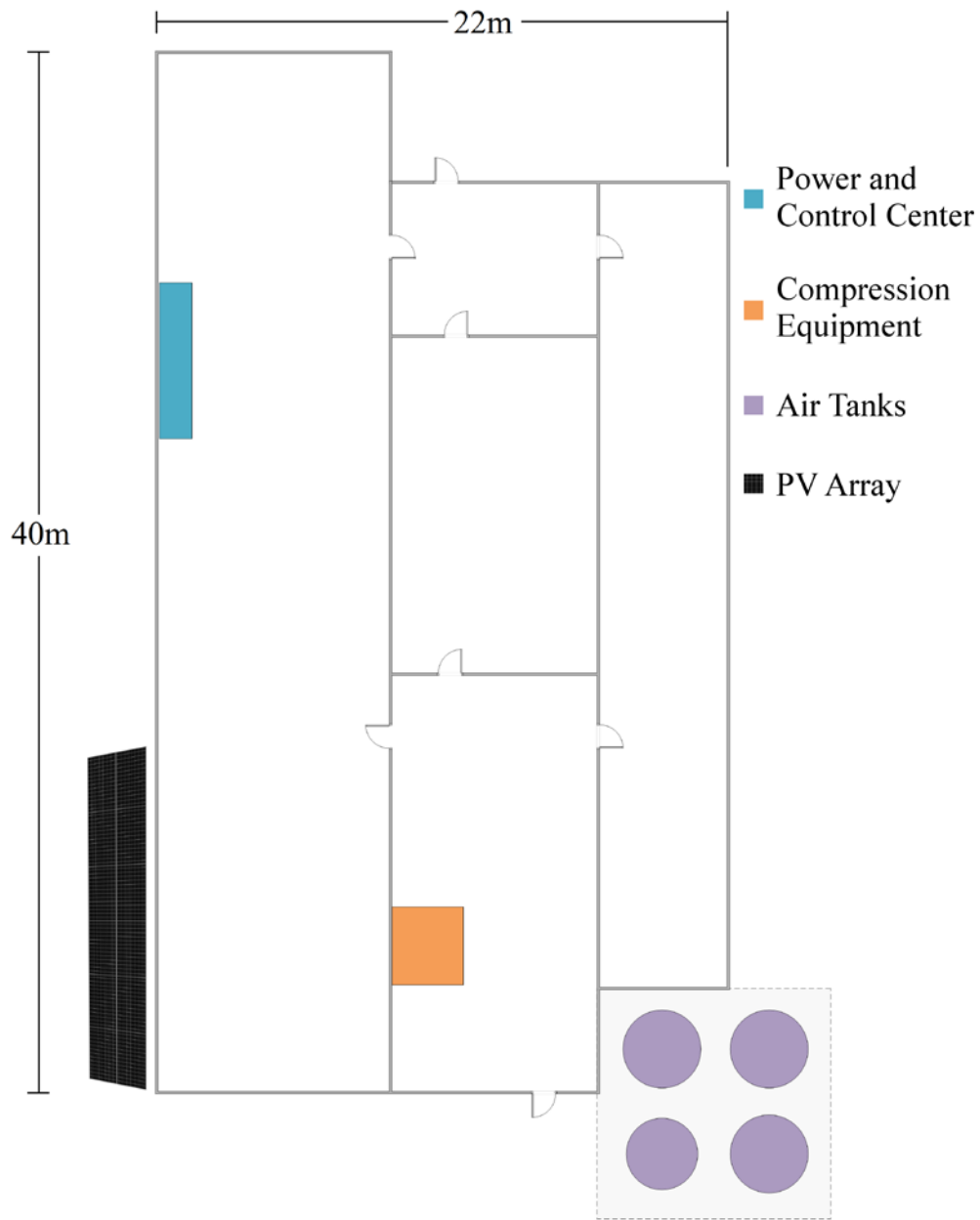
Figure 22.   NPS IMPEL Building Layout

B. TESTING

The completion of several tests was required to validate the control system functionality. Due to the limitations of the inverter, as previously discussed, the testing had to be started manually. To allow for proper system response, the inverter breaker was not switched on until the capacitor bank voltage above 31 VDC to keep the inverter from entering self-protect mode. Through testing, it was determined that the capacitor voltage was required to remain greater than 30 VDC for 15 minutes prior to turning on the breaker. This setup method provided the most realistic simulation of an automatable inverter. The data shown in Figure 23 starts at approximately 7:35 AM; however, the data for this run was collected on May 1, 2017 when the sunrise occurred at 6:14 AM [57]. This indicates that it was approximately 75 minutes after sunrise until the capacitors reached a voltage capable of running the inverter and compressor.
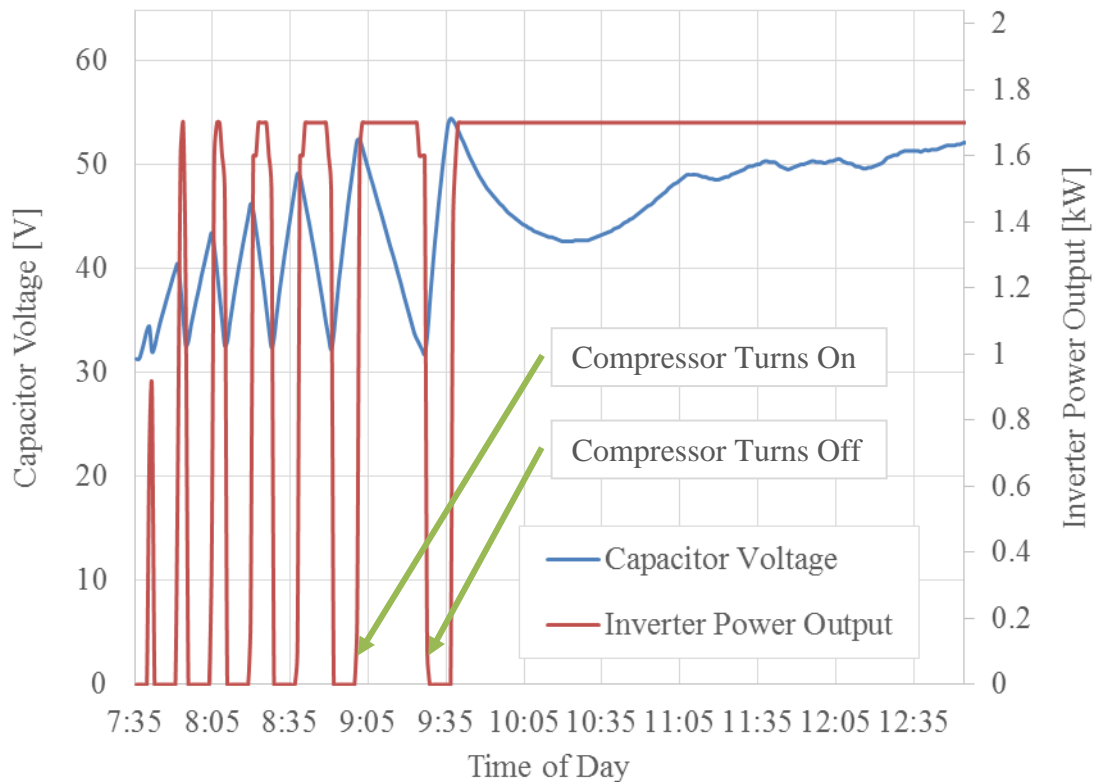
Figure 23.   Sunrise Compressor Run Data

As Figure 23 shows, the compressor runs for short periods, reducing capacitor voltage to the compressor shut-off point six times over the course of approximately 120 minutes. During this time, the compressor ran for approximately 56 minutes, or just short of half the time. Following the compressor start that occurred at approximately 9:35, there is a significant dip in capacitor voltage, indicating that the incident solar radiance was not quite enough to compensate for the running compressor. However, the solar radiance incident upon the PV array eventually produced enough power to compensate for the running compressor, preventing further automatic shutoffs during this data run. The data shows that the system is capable of automatic operation, as intended.

IV.   CONCLUSIONS AND RECOMMENDATIONS

The purpose of this research was to develop and implement an automated control system for the SS-CAES compression cycle. Achieving this goal required a combination of monitoring available solar radiance and available temporary power to ensure the system was maximizing available runtimes. By demonstrating the functionality of this system, the NPS IMPEL is now capable of producing compressed air from a purely renewable source. Additionally, this project will result in significant energy savings for future supersonic wind tunnel testing, as it maintains the air tanks at 33% of required capacity. This project, when combined with a compressed air generator, paves the way for a complete SS-CAES system. Implementing more systems similar to this SS-CAES system across military installations will reduce reliance on fossil fuels and greatly enhance the renewable energy profile of the DOD.

The following sections contain recommendations for future enhancement of the NPS IMPEL SS-CAES system.

(1)   Fully Automated Inverter

The voltage limitations and lack of automatic restart of the Sunny Island inverter presented an insurmountable obstacle during this project. Specifically, the issue of inverter's self-protect mode and subsequent physical switch manipulation to enable restarting was not solved. While thought was given to implementing a linear actuator to automatically manipulate the breaker, it was determined that automatic operation of a safety device was potentially unsafe and therefore not performed. However, three possible solutions exist for this problem. The first would be to replace the Sunny Island inverter completely with one that does not enter a self-protect mode at low input voltages. By installing an inverter that is also capable of producing 240 VAC directly, the Smartformer could also be eliminated, further increasing system efficiency. The second possible solution would be to add more temporary energy storage to ensure that the input voltage to the Sunny Island inverter never drops below the required 30 VDC after the sun sets. This would likely require the installation of an additional 12 ultracapacitors, for a

usable system storage capability of 653 Wh. The third possible solution, and likely the most effective, is explored further in the next section.

(2)   Combine SS-CAES Compression and Expansion

By combining the SS-CAES compression and expansion systems together, it would be possible to negate any issues with the Sunny Island inverter. Specifically, by having the expansion system maintain voltage on the capacitor bank at or above the minimum required for inverter operation, true automation can be accomplished. Additionally, the control systems for the compression and expansion systems are virtually identical [18]. This would allow further automation and integration with each other.

(3)   Implement TES for Improved Efficiency

Using TES, as in the case of the ADELE Project, would further increase the system efficiency. This would allow the NPS IMPEL SS-CAES system to more closely approximate a system with isothermal expansion, which results in nearly twice the energy storage per unit volume within the air tanks.

APPENDIX A. TANK VOLUME AND ENERGY CALCULATIONS

```matlab
%% CAES Tank Volume & Energy Determination MATLAB Code
%   Joshua Williams

%% Tank Volume Determiniation

clc; close all; clear all;

% Number of tanks
tanks = 3;

% Outer Tank Diameter
D = 10*2.54*12/100; % m

% Overall Height
ht_oa = 23.5*2.54*12/100; % m

% Outer Radius of Cylinder
r_cyl_out = D/2; % m

% Cylinder to End Cap Radius Ratio
r_ratio = 1/2;

% Outer Radius of End Caps
r_end_out = r_cyl_out * r_ratio; % m

% Thickness of Cylinder
th_cyl = 1.125*2.54/100; % m

% Inner Radius of Cylinder
r_cyl_in = r_cyl_out - 2 * th_cyl; % m

% Height of Cylinder Portion
ht_cyl = ht_oa-2*r_end_out; % m

% Volume of Cylinder Portion
V_cyl = pi * r_cyl_in^2 * ht_cyl; % m^3

% Thickness of End Caps
th_end = 1.148*2.54/100; % m

% Inner Radius of End Caps
r_end_in = r_end_out - 2 * th_end; % m
```

```matlab
% Volume of Ellipsoidal End Caps (combined)
V_ends = 4/3 * pi * r_cyl_in^2 * r_end_in; % m^3

% Volume of One Tank:
Vol_one = V_cyl + V_ends; % m^3

% Volume of all Tanks:
Vol_tot = Vol_one * tanks; % m^3

%% Energy Content of Tanks

% Tank Pressure
P1 = 792.897; % kPa

% Atmospheric Pressure
P2 = 101.325; % kPa

% Tank Volume (from above)
V1 = Vol_tot; % m^3

% Ambient Temperature
T1 = 293; % K

% Constant Pressure Specific Heat
Cp = 1.004; % kJ/kg-K

% Constant Volume Specific Heat
Cv = 0.717; % kJ/kg-K

% Specific Heat Ratios
gamma = Cp/Cv;

% Ideal Gas Constant
R = Cp-Cv;

% Volume After Isothermal Expansion
V2_iso = P1*V1/P2; % m^3

% Isothermal Work
W_iso = P1*V1 * log(P1/P2); % kJ

% Isothermal Temperature (no change)
T2_iso = T1; % K

% Isothermal Work in kWh
W_iso_kWh = W_iso/3600 % kWh
```

```matlab
% Volume After Adiabatic Expansion
V2_ad = ((P1*V1^gamma)/P2)^(1/gamma); % m^3

% Adiabatic Work
W_ad = (P2*V2_ad-P1*V1)/(1-gamma); % kJ

% Adiabatic Exit Temperature
T2_ad = T1*(P2/P1)^((gamma-1)/gamma); % K

% Adiabatic Work in kWh
W_ad_kWh = W_ad/3600 % kWh
```

THIS PAGE INTENTIONALLY LEFT BLANK

APPENDIX B. CONTROLLER SOFTWARE SETUP

This appendix covers obtaining the supporting software for programming the PLC and HMI. The software for programming the PLC and HMI is called Rockwell Automation Connected Components Workbench. It can be obtained from the downloads section at the following web address: http://rockwellautomation.com/global/support/connected-components/workbench.page. The user may be required to create an account to download the software, but the standard edition of the software is free of charge. Connected Components Workbench version 9 was used to program the PLC and HMI for the SS-CAES compression system. The user is required to have administrator privileges on the PC to complete the installation. The installation requires approximately 5 GB of storage space on the hard drive.

THIS PAGE INTENTIONALLY LEFT BLANK

APPENDIX C. CONTROLLER PROGRAM.

This appendix contains all settings and programs that run on the Micro850 Controller. The intent is that the reader will be able to take this information and fully recreate the control system.

A.   CONTROLLER WIDE SETTINGS

This section contains all controller settings, global variables, and user-defined data types.

1.   Settings

Table 2   Settings

Setting	Value
Controller	
General	
Name:	AutomatedCAES
Ethernet	
Configure IP address and settings	Selected
IP Address:	192.168.0.1
Subnet Mask	255.255.255.0
Gateway Address	192.168.0.0

2. Global Variables

Table 3 Global Variables

Name	Data Type	Initial Value
allow_inverter_off	BOOL	TRUE
allow_inverter_on	BOOL	FALSE
batt_abs_min	WORD	310
batt_min_start	WORD	325
batt_voltage_abs_min	REAL	31.0
batt_voltage_min_start	REAL	33.0
batt_voltage_min_stop	REAL	32.0
battery_status_charged	BOOL	FALSE
battery_voltage	REAL	
battery_voltage_max	REAL	53.0
battery_voltage_min_restart	REAL	40.0
button_visible	BOOL	
cmd_start_compressor	BOOL	
cmd_start_inverter	BOOL	
cmd_stop_compressor	BOOL	
cmd_stop_inverter	BOOL	
compressor_allow_restart	BOOL	TRUE
compressor_run_today	BOOL	FALSE
compressor_running	BOOL	FALSE
compressor_status	UINT	
day	UINT	
day_run	UINT	1
error_charger_modbus	BOOL	FALSE
error_inverter_modbus	BOOL	FALSE
HeartBeat	BOOL	
hour	UINT	
inverter_recent_off	BOOL	FALSE
inverter_status_online	BOOL	
inverter_status_running	BOOL	FALSE
ManualControlEnabled	BOOL	
min_restart_time	REAL	10.0
minute	UINT	
modbus_offset	UDINT	1
month	UINT	
month_run	UINT	1
pv_abs_min	WORD	500
pv_min_start	WORD	550
pv_voltage	REAL	

Name	Data Type	Initial Value
pv_volts_min	REAL	50.0
pv_volts_min_start	REAL	55.0
relay_on	BOOL	FALSE
sun_is_up	BOOL	FALSE
today	RISE_SET_TIME	
rise_hr	UINT	
rise_min	UINT	
set_hr	UINT	
set_min	UINT	

3. User-Defined Data Types

Table 4   User-Defined Structure Data Type

Name	Data Type
RISE_SET_TIME	RISE_SET_TIME
rise_hr	UINT
rise_min	UINT
set_hr	UINT
set_min	UINT

B. PROGRAMS

The programs for the Allen-Bradley Micro850 are either Function Block Diagram (FBD) form, or Structured Text form.

1. StartupReset

This FBD program resets global variables to the values required to prevent undesired operation. This program only runs once at the beginning of the first loop following power on.

a. *Function Block Diagram*
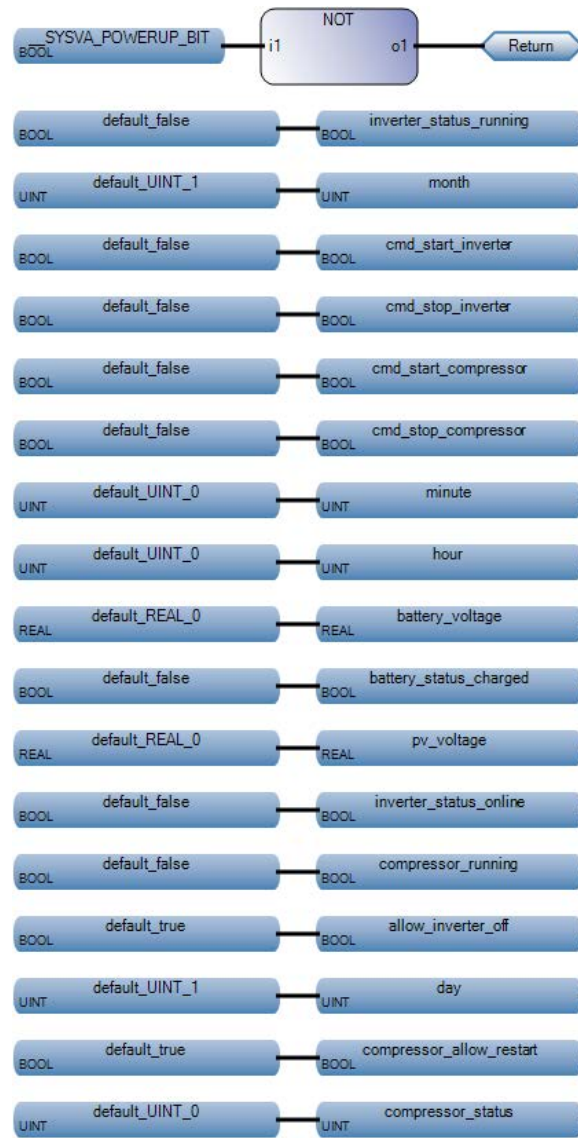
Figure 24.   StartupReset FBD

Table 5   StartupReset Local Variables

Name	Data Type	Initial Value	Attribute
default_false	BOOL	FALSE	Read
default_REAL_0	REAL	0.0	Read
default_true	BOOL	TRUE	Read
default_UINT_0	UINT	0	Read
default_UINT_1	UINT	1	Read

2.   UpdateSettings

This FBD program converts user-defined voltage set points for use later in the control loop. Additionally, this program performs checks to see if 1) the compressor has run today and 2) whether the inverter start and stop buttons should be visible on the HMI.

a. *Function Block Diagram*
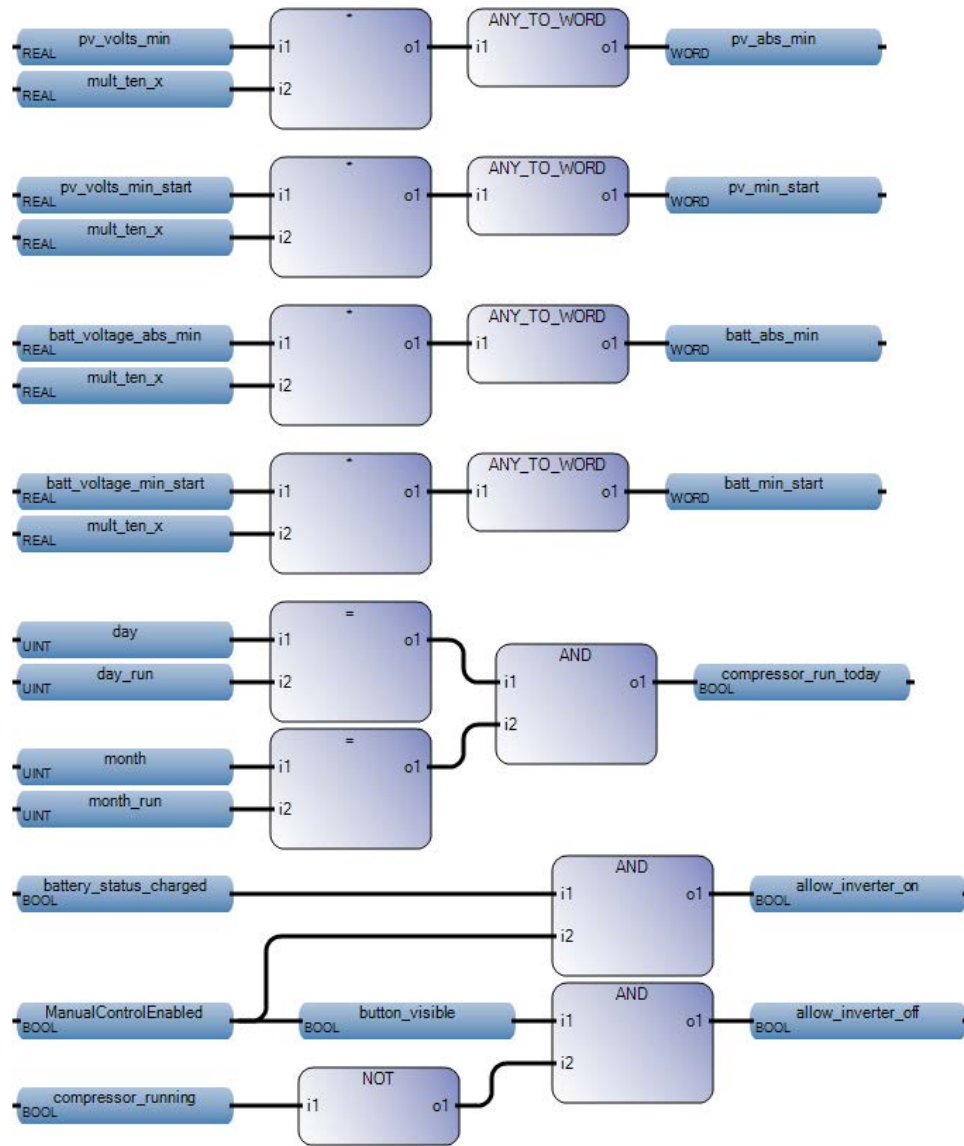
Figure 25.   UpdateSettings FBD

b. *Local Variables*

Table 6   UpdateSettings Local Variables

Variable Name	Data Type	Initial Value
mult_ten_x	REAL	10.0

3. ProgHeartbeat

This FBD program provides a graphical indication of connectivity between the controller and the HMI.

a. *Function Block Diagram*
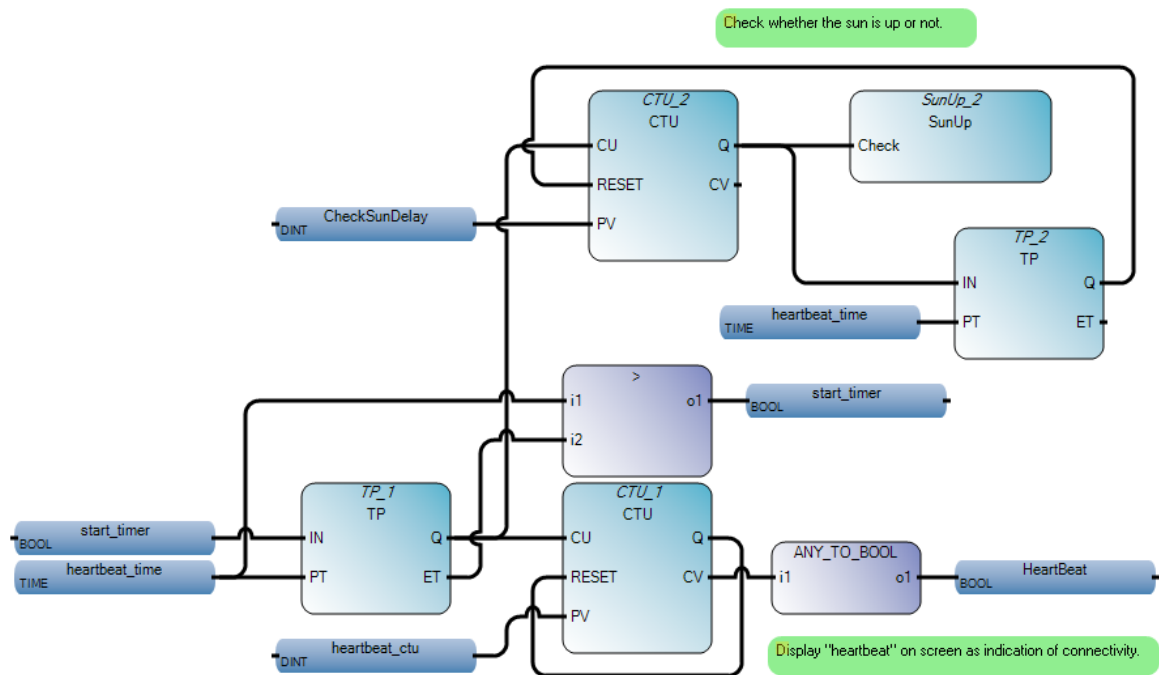
Figure 26.　Heartbeat Program Function Block Diagram

b. *Local Variables*

Table 7　Heartbeat Local Variables

Variable Name	Data Type	Initial Value
CheckSunDelay	DINT	60
heartbeat_ctu	DINT	2
heartbeat_time	Time	T#1s
start_timer	BOOL	TRUE

4. VerifySunState

This FBD program retrieves PV array voltage and capacitor voltage from the MidNite Classic 150 charge controller via Modbus. Comparing these values to set points ensures that there is sufficient sunlight (in the form of PV voltage) and charge (in the form of capacitor voltage) to run the equipment. Additionally, this FBD checks the status of the drop-out relay, to determine the proper indication to display for the status of the compressor while running.

a. Function Block Diagram
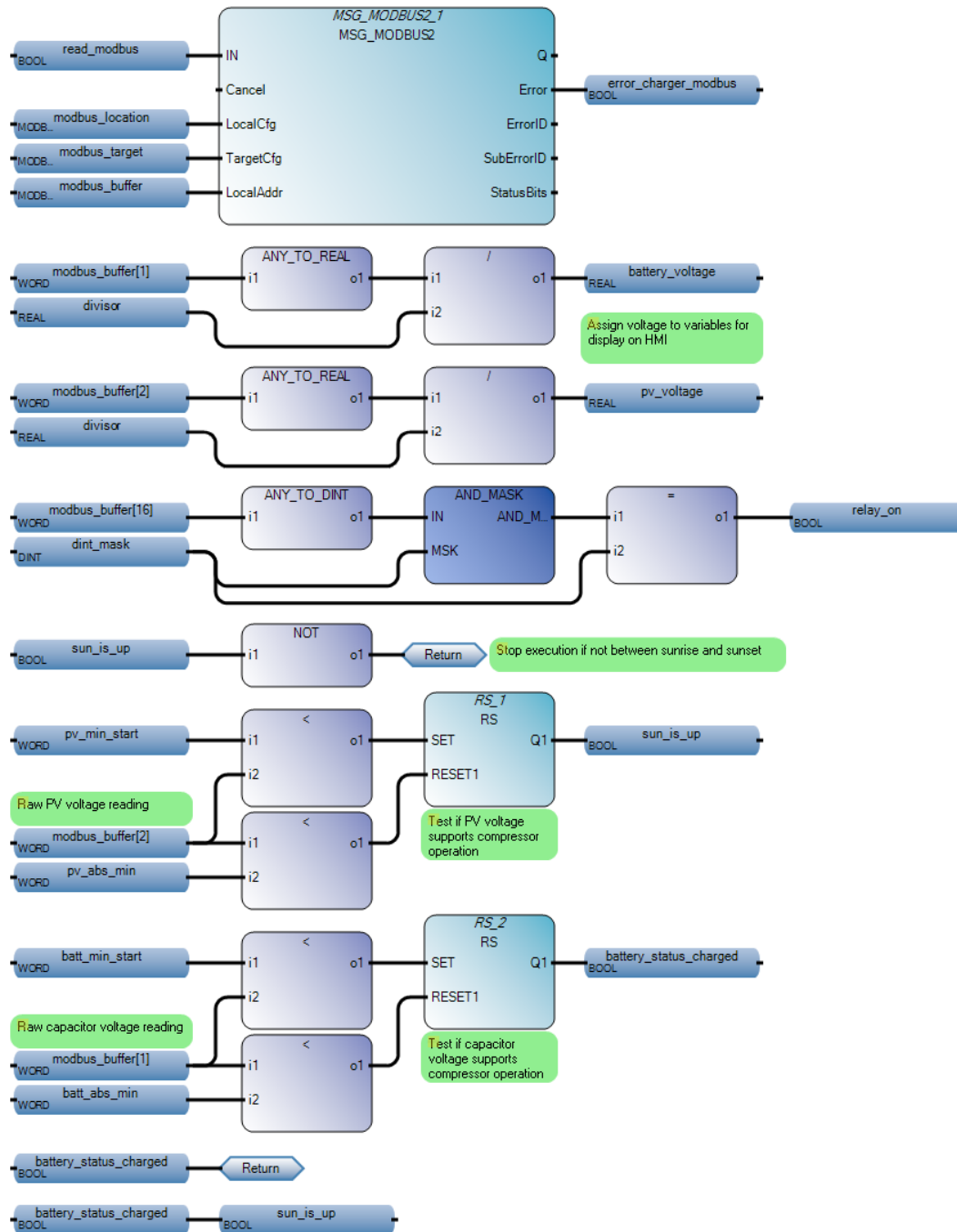
Figure 27.   VerifySunState FBD

Table 8   VerifySunState Local Variables

Variable Name	Data Type	Initial Value
dint_mask	DINT	16384
divisor	REAL	10.0
modbus_buffer	MODBUSLOCADDR	
modbus_location	MODBUS2LOCPARA	
Channel	UINT	4
TriggerType	UDINT	10000
Cmd	USINT	3
ElementCnt	UINT	2
modbus_target	MODBUS2TARPARA	
Addr	UDINT	4115
NodeAddress	MODBUS2NODEADDR	
NodeAddress[0]	USINT	192
NodeAddress[1]	USINT	168
NodeAddress[2]	USINT	0
NodeAddress[3]	USINT	50
Port	UINT	0
UnitId	USINT	1
MsgTimeout	UDINT	0
ConnTimeout	UDINT	0
ConnClose	BOOL	TRUE
read_modbus	BOOL	TRUE

5.   CompressorRestartDelay

This FBD program sets a bit to ensure the compressor is off for a user-defined length of time prior to restarting.
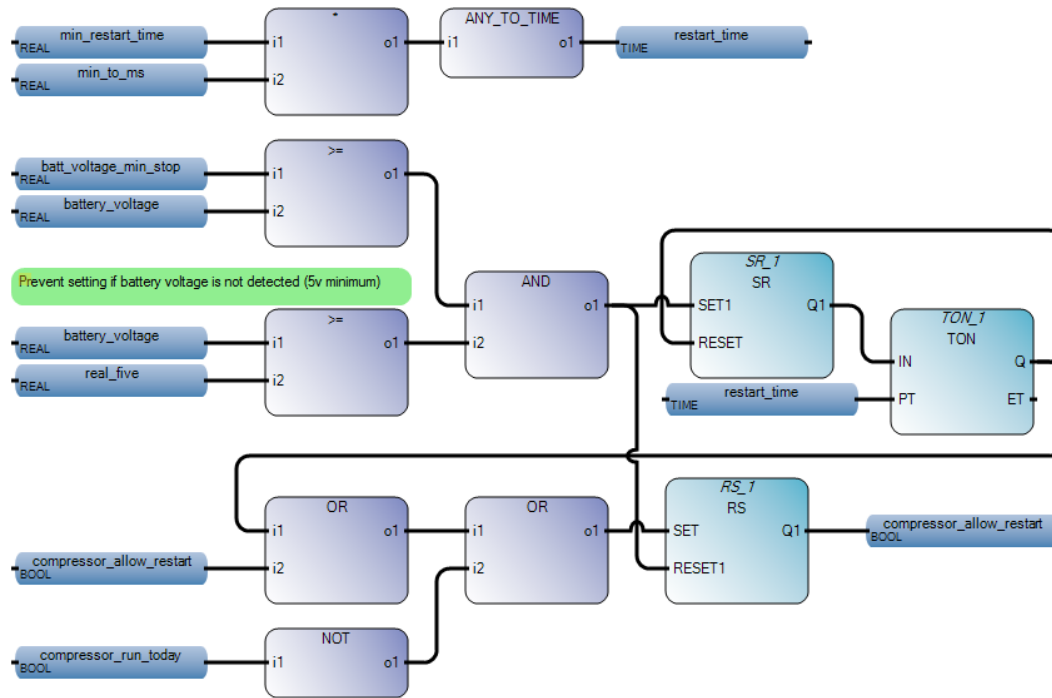
Figure 28.   CompressorRestartDelay FBD

b. *Local Variables*

Table 9   CompressorRestartDelay Local Variables

Variable Name	Data Type	Initial Value
min_to_ms	REAL	60000.0
real_five	REAL	5.0
restart_time	TIME	T#10m

6.   CheckInverterStatus

This FBD program checks if the inverter has power and if it is running.

55

a. ***Function Block Diagram***
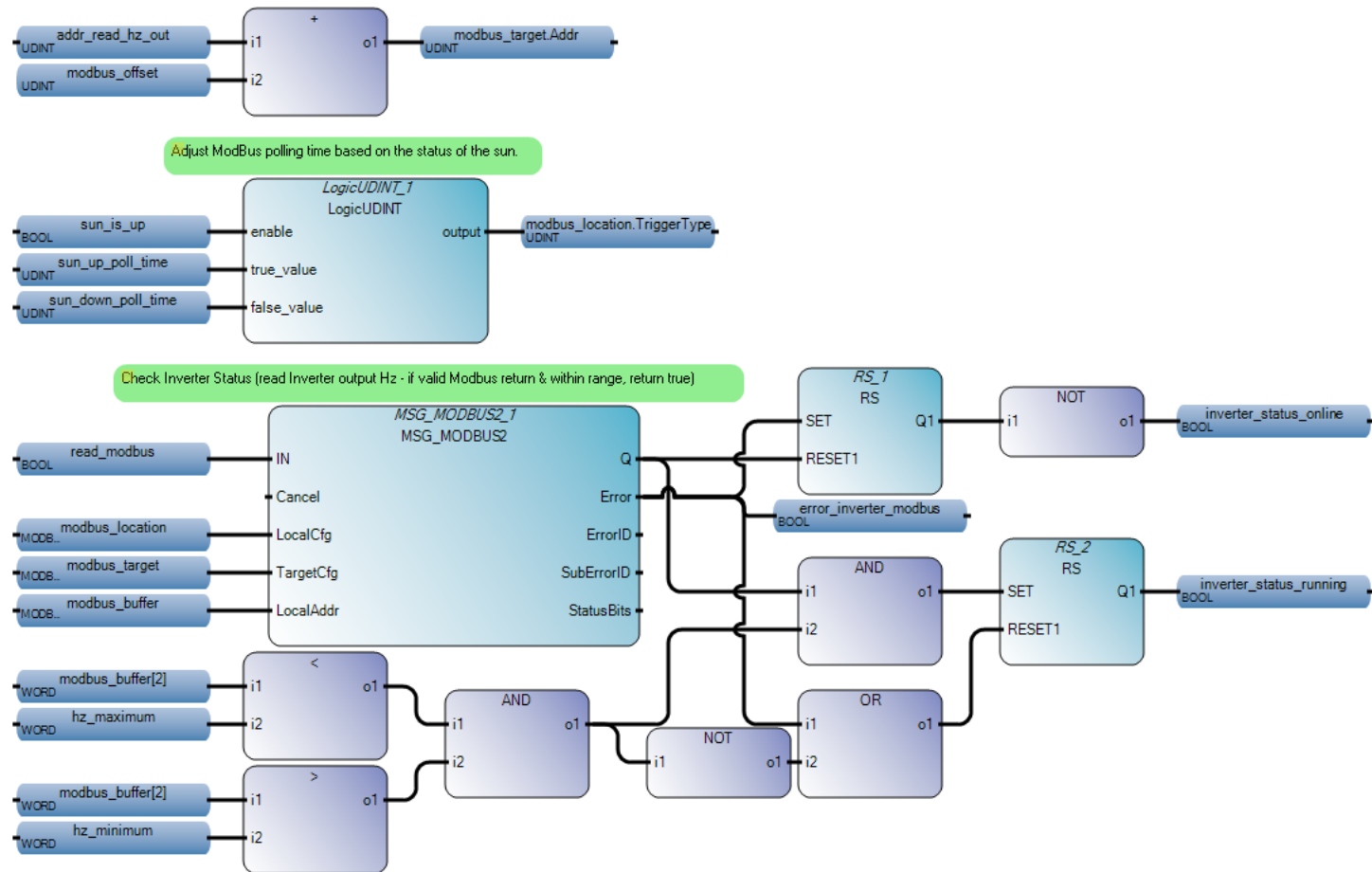
Figure 29.   CheckInverterStatus FBD

Table 10   CheckInverterStatus Local Variables

Variable Name	Data Type	Initial Value
modbus_location	MODBUS2LOCPARA	
Channel	UINT	4
TriggerType	UDINT	10000
Cmd	USINT	4
ElementCnt	UINT	2
modbus_target	MODBUS2TARPARA	
Addr	UDINT	30058
NodeAddress	MODBUS2NODEADDR	
NodeAddress[0]	USINT	192
NodeAddress[1]	USINT	168
NodeAddress[2]	USINT	0
NodeAddress[3]	USINT	168
Port	UINT	0
UnitId	USINT	3
MsgTimeout	UDINT	0
ConnTimeout	UDINT	0
ConnClose	BOOL	TRUE
modbus_buffer	MODBUSLOCADDR	
read_modbus	BOOL	TRUE
sun_up_poll_time	UDINT	10000
sun_down_poll_time	UDINT	60000
addr_read_hz_out	UDINT	30803
hz_minimum	WORD	5800
hz_maximum	WORD	6200

7.   InverterOffHold

This FBD program forces the controller to treat the inverter as switched off after either an automatic or a manual shutdown of the inverter. This is required as there is an approximately 30 second delay between inverter status change and inverter status update via the Sunny WebBox.

a. ***Function Block Diagram***
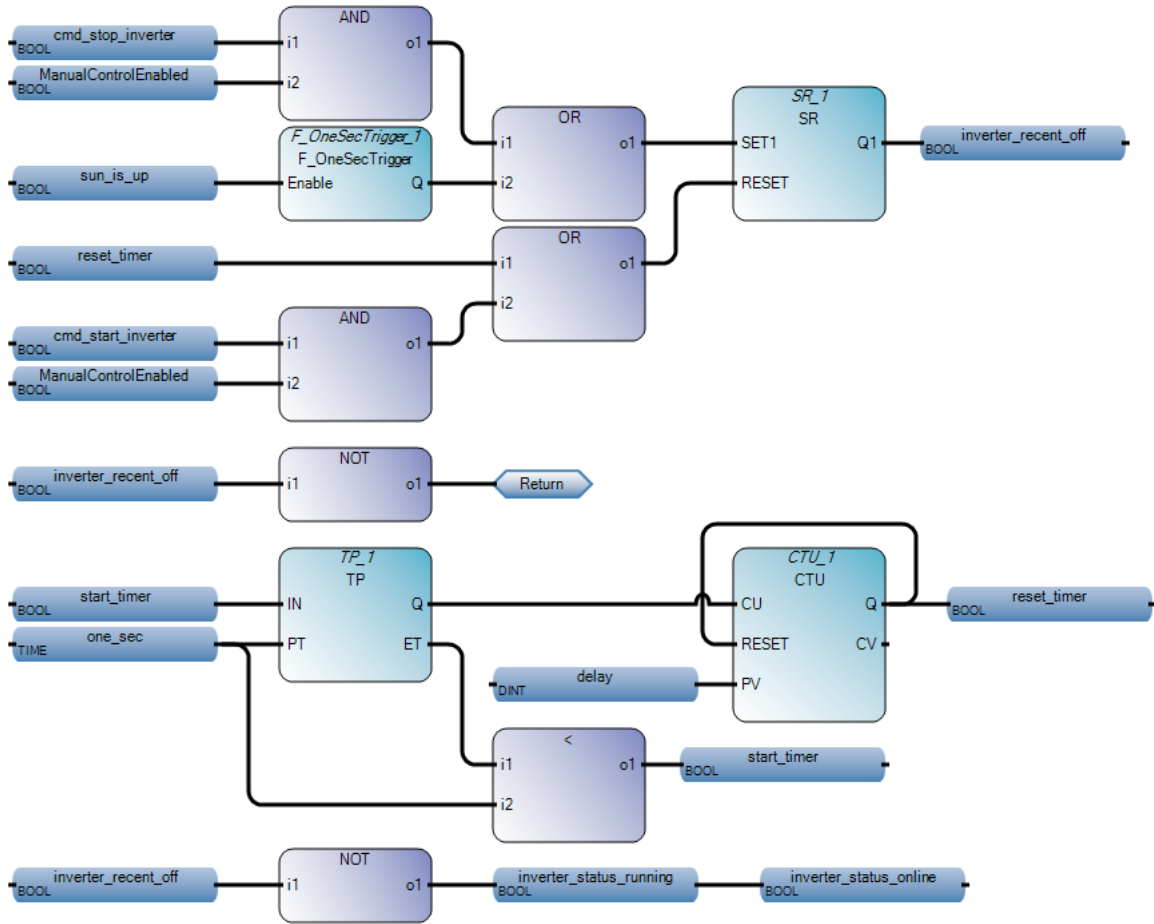
Figure 30. InverterOffHold FBD

b. ***Local Variables***

Table 11 InverterOffHold Local Variables

Variable Name	Data Type	Initial Value
start_timer	BOOL	TRUE
one_sec	TIME	T#1s
delay	DINT	45
reset_timer	BOOL	FALSE

8. AutomaticInverterControl

This FBD program automatically starts and stops the inverter based on the available power.

a. *Function Block Diagram*
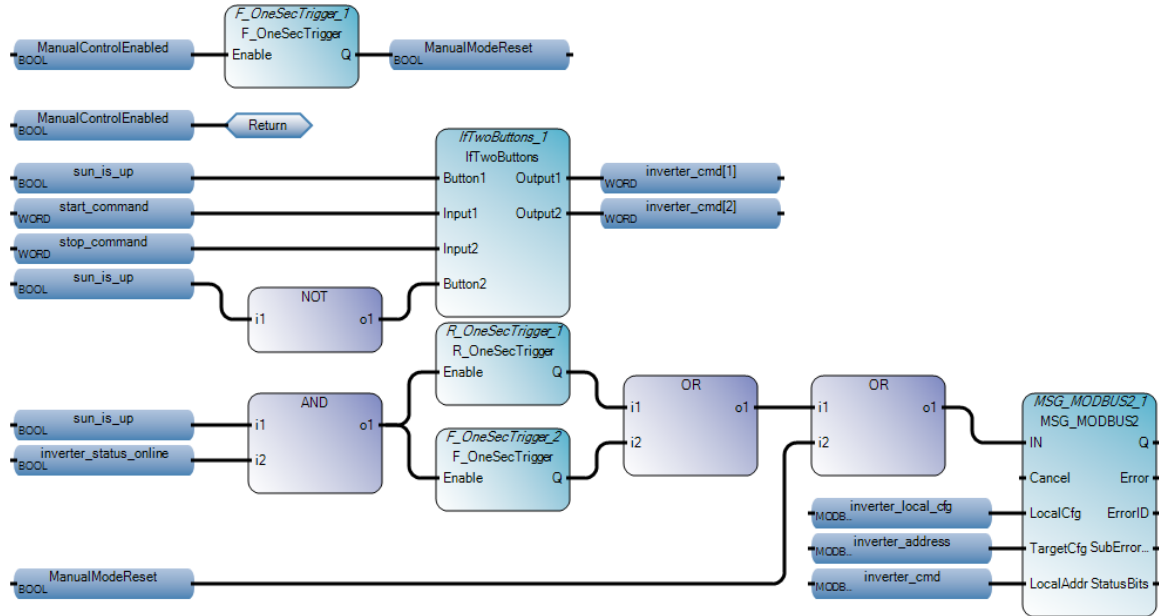
Figure 31.   AutomaticInverterControl FBD

Table 12   AutomaticInverterControl Local Variables

Variable Name	Data Type	Initial Value
inverter_local_cfg	MODBUS2LOCPARA	
Channel	UINT	4
TriggerType	UDINT	0
Cmd	USINT	16
ElementCnt	UINT	2
inverter_address	MODBUS2TARPARA	
Addr	UDINT	40010
NodeAddress	MODBUS2NODEADDR	
NodeAddress[0]	USINT	192
NodeAddress[1]	USINT	168
NodeAddress[2]	USINT	0
NodeAddress[3]	USINT	168
Port	UINT	0
UnitId	USINT	3
MsgTimeout	UDINT	0
ConnTimeout	UDINT	0
ConnClose	BOOL	TRUE
inverter_cmd	MODBUSLOCADDR	
start_command	WORD	569
stop_command	WORD	381
ManualModeReset	BOOL	FALSE

9.   ManualInverterControl

This FBD program allows for manual control of the inverter.
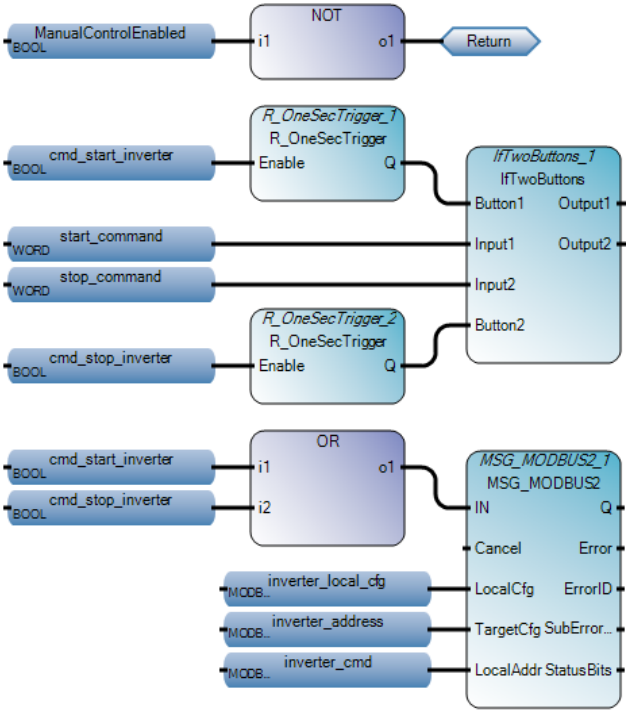
Figure 32.   ManualInverterControl FBD

Table 13   ManualInverterControl Local Variables

Variable Name	Data Type	Initial Value
inverter_local_cfg	MODBUS2LOCPARA	
Channel	UINT	4
TriggerType	UDINT	0
Cmd	USINT	16
ElementCnt	UINT	2
inverter_address	MODBUS2TARPARA	
Addr	UDINT	40010
NodeAddress	MODBUS2NODEADDR	
NodeAddress[0]	USINT	192
NodeAddress[1]	USINT	168
NodeAddress[2]	USINT	0
NodeAddress[3]	USINT	168
Port	UINT	0
UnitId	USINT	3
MsgTimeout	UDINT	0
ConnTimeout	UDINT	0
ConnClose	BOOL	TRUE
inverter_cmd	MODBUSLOCADDR	
start_command	WORD	569
stop_command	WORD	381

10.   AutomaticCompressorControl

This FBD program automatically starts and stops the compressor and air dryer based on the available power.

a. *Function Block Diagram*
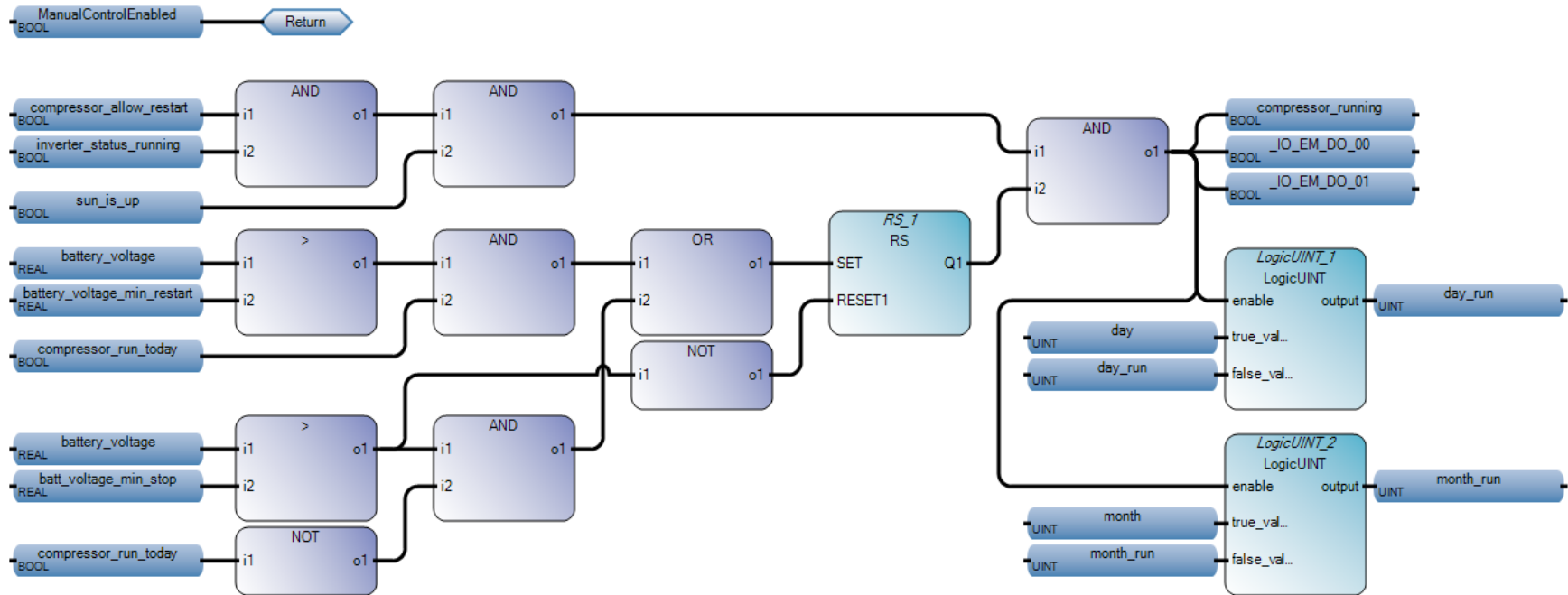
Figure 33.   AutomaticCompressorControl FBD

63

There are no local variables for the program AutomaticCompressorControl.

11. ManualCompressorControl

This FBD program allows for manual control of the compressor and air dryer.

a. *Function Block Diagram*
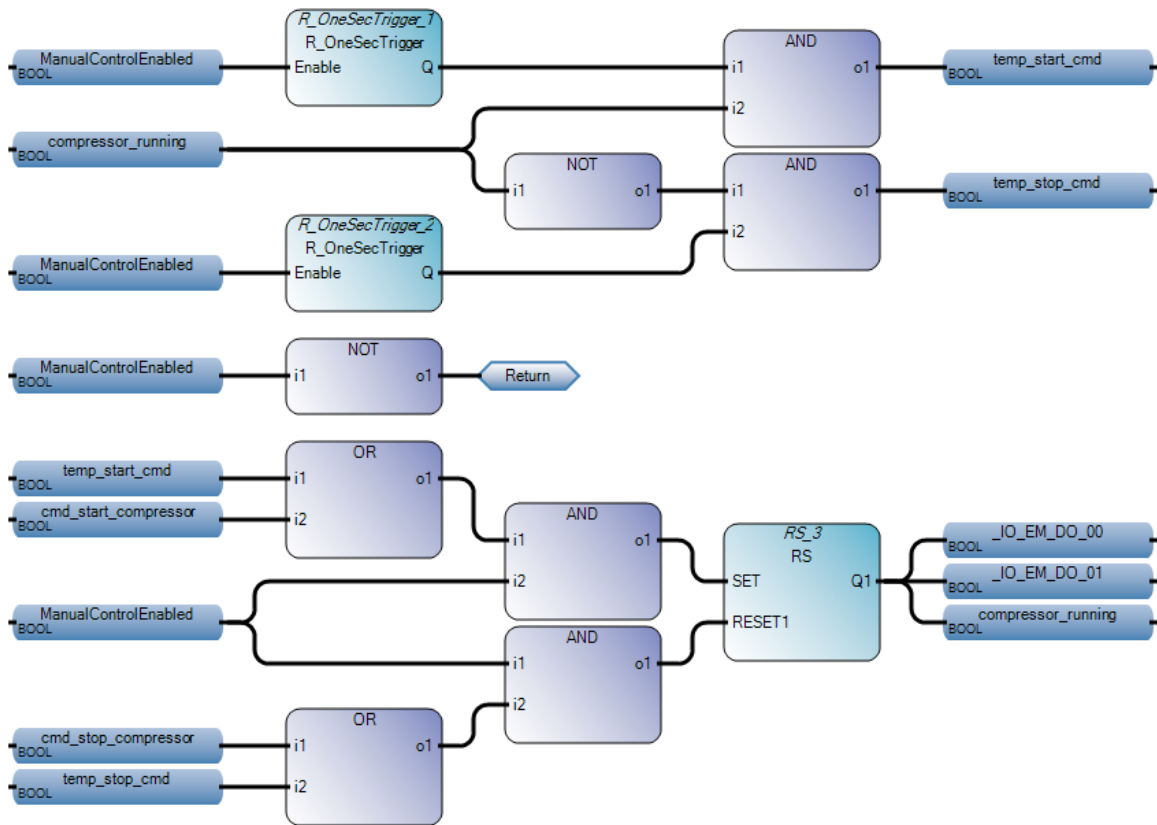
Figure 34.   ManualCompressorControl FBD

b. *Local Variables*

Table 14   ManualCompressorControl Local Variables

Variable Name	Data Type	Initial Value
temp_start_cmd	BOOL	FALSE
temp_stop_cmd	BOOL	FALSE

12. UpdateCompressorState

This FBD program checks the power output of the inverter to determine if the compressor is running from the inverter since there is no direct indication of the compressor running.

a. Function Block Diagram
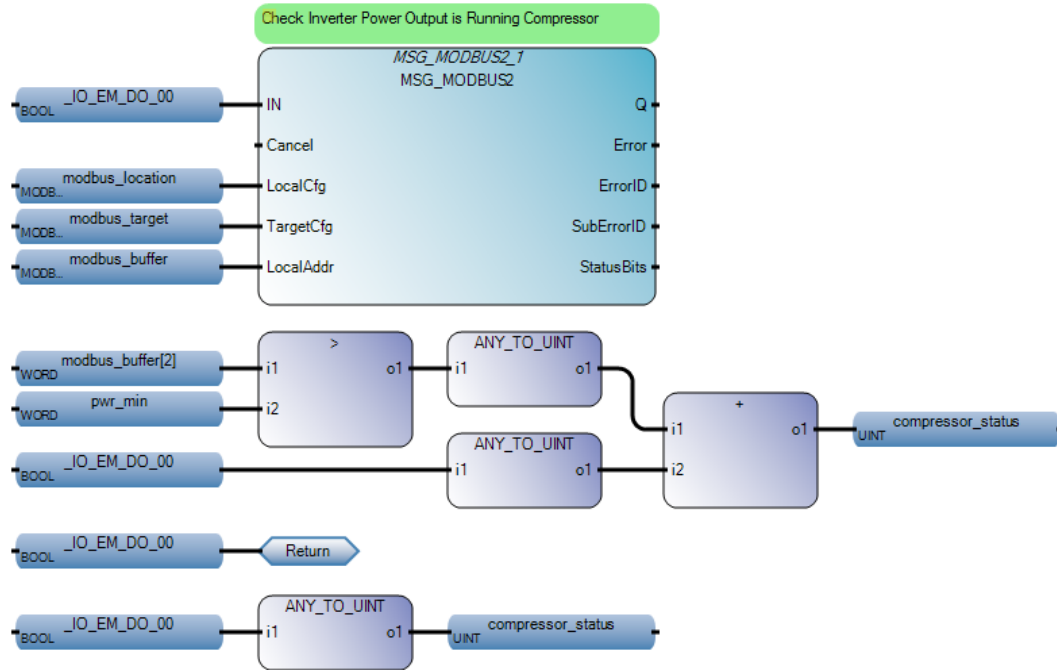
Figure 35.   UpdateCompressorState FBD

b. Local Variables

Table 15   UpdateCompressorState Local Variables

Variable Name	Data Type	Initial Value
pwr_min	WORD	1000

C. USER-DEFINED FUNCTION BLOCKS

In some instances, a function does not exist that will perform the desired function. In these cases, the user must create a function in the User-Defined Function Blocks

portion of the Connected Components Workbench (CCW) software. This section describes those functions.

1. SunUp

This Structured Text style User-Defined Function Block checks against a table of sunrise and sunset times to determine if the sun is available for energy production.

a. Structured Text

```
IF Check THEN
    CASE month OF
         1 : today  := jan;
         2 : today  := feb;
         3 : today  := mar;
         4 : today  := apr;
         5 : today  := may;
         6 : today  := jun;
         7 : today  := jul;
         8 : today  := aug;
         9 : today  := sep;
         10: today  := oct;
         11: today  := nov;
         12: today  := dec;
    END_CASE;
    (* Check to see if the sun is up *)
    IF (hour > today.rise_hr OR (hour = today.rise_hr
 AND minute > today.rise_min)) THEN
         IF (hour < today.set_hr OR (hour = today.set_hr
 AND minute < today.set_min)) THEN
             sun_is_up := TRUE;
         ELSE
             sun_is_up := FALSE;
         END_IF;
    ELSE
         sun_is_up := FALSE;
    END_IF;
END_IF;
```

Table 16   SunUp Local Variables

Name	Data Type	Value	Name	Data Type	Value
jan	RISE_SET_TIME		jul	RISE_SET_TIME	
rise_hr	UINT	7	rise_hr	UINT	5
rise_min	UNIT	20	rise_min	UNIT	13
set_hr	UINT	17	set_hr	UINT	19
set_min	UINT	03	set_min	UINT	14
feb	RISE_SET_TIME		aug	RISE_SET_TIME	
rise_hr	UINT	7	rise_hr	UINT	5
rise_min	UNIT	9	rise_min	UNIT	38
set_hr	UINT	17	set_hr	UINT	18
set_min	UINT	34	set_min	UINT	37
mar	RISE_SET_TIME		sep	RISE_SET_TIME	
rise_hr	UINT	6	rise_hr	UINT	6
rise_min	UNIT	38	rise_min	UNIT	2
set_hr	UINT	18	set_hr	UINT	17
set_min	UINT	2	set_min	UINT	52
apr	RISE_SET_TIME		oct	RISE_SET_TIME	
rise_hr	UINT	5	rise_hr	UINT	6
rise_min	UNIT	53	rise_min	UNIT	30
set_hr	UINT	18	set_hr	UINT	17
set_min	UINT	30	set_min	UINT	11
may	RISE_SET_TIME		nov	RISE_SET_TIME	
rise_hr	UINT	5	rise_hr	UINT	7
rise_min	UNIT	14	rise_min	UNIT	1
set_hr	UINT	18	set_hr	UINT	16
set_min	UINT	56	set_min	UINT	52
jun	RISE_SET_TIME		dec	RISE_SET_TIME	
rise_hr	UINT	4	rise_hr	UINT	7
rise_min	UNIT	53	rise_min	UNIT	20
set_hr	UINT	19	set_hr	UINT	16
set_min	UINT	21	set_min	UINT	52

2.   **IfTwoButtons**

This Structured Text style User-Defined Function Block provides a specified output based on an input TRUE value. This function is used to specify whether the start or stop command for the Sunny Island inverter should be sent via Modbus.

a.   *Structured Text*

```
IF Button1 THEN
     Output1 := 0;
     Output2 := Input1;
ELSE
     Output1 := 0;
     Output2 := Input2;
END_IF;
```

b.   *Local Variables*

Table 17   IfTwoButtons Local Variables

Name	Data Type	Direction
Button1	BOOL	VarInput
Input1	WORD	VarInput
Input2	WORD	VarInput
Button2	BOOL	VarInput
Output1	WORD	VarOutput
Output2	WORD	VarOutput

3.   LogicUDINT

This Structured Text style User-Defined Function Block adjusts its UDINT output based on a single Boolean input. It is used to adjust the time between inverter status checks based upon the status of the sun.

a.   *Structured Text*

```
IF enable THEN
     output  := true_value;
ELSE
     output  := false_value;
END_IF;
```

b.   *Local Variables*

Table 18   LogicUDINT Local Variables

Name	Data Type	Direction
enable	BOOL	VarInput
true_value	UDINT	VarInput
false_value	UDINT	VarInput
output	UDINT	VarOutput

4.   **LogicUINT**

This Structured Text style User-Defined Function Block is identical to LogicUDINT with the exception that all local variables of UDINT data type are now UINT data types.

5.   **F_OneSecTrigger**

This FBD style User-Defined Function Block modifies the provided falling-edge trigger and maintains the output for a duration of one second. This longer trigger time is required for condition based Modbus queries to succeed.

a.   *Function Block Diagram*
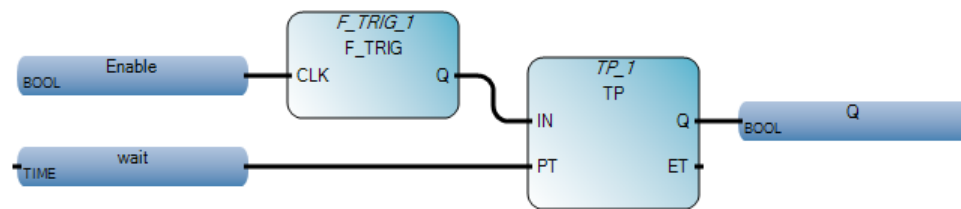
Figure 36.   F_OneSecTrigger FBD

Table 19   F_OneSecTrigger Local Variables

Name	Data Type	Initial Value	Direction
Enable	BOOL		VarInput
Q	BOOL		VarOutput
wait	TIME	T#1s	Var

6.   R_OneSecTrigger

This FBD style User-Defined Function Block modifies the provided rising-edge trigger and maintains the output for a duration of one second. This longer trigger time is, again, required for condition based Modbus queries to succeed.

a.   *Function Block Diagram*
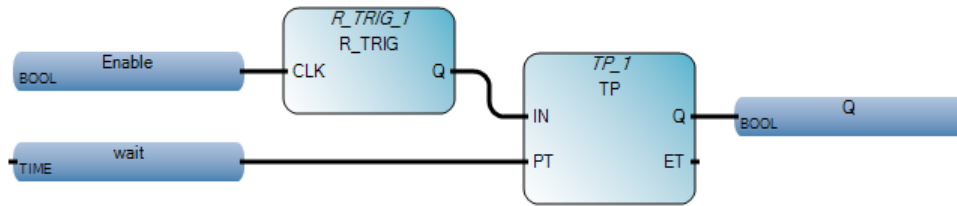
Figure 37.   R_OneSecTrigger FBD

b.   *Local Variables*

Table 20   R_OneSecTrigger Local Variables

Name	Data Type	Initial Value	Direction
Enable	BOOL		VarInput
Q	BOOL		VarOutput
wait	TIME	T#1s	Var

70

APPENDIX D. SCREEN PROGRAM

This appendix covers the both the settings changed on the HMI directly, as well as the HMI program that was created in Connected Components Workbench.

A.   NETWORK SETUP

The network setup was conducted from the screen of the HMI. By accessing the "Main" screen, and setting the values as indicated in Table 21.

Table 21   HMI Network Setup

Setting Name	Value
Main	
Communication	
Set Static IP Address	
IP Address	192.168.0.2
Mask	255.255.255.0
Gateway	192.168.0.1

B. TAGS

Table 22   External Tags

Tag Name	Data Type	Address
AllowInvOff	Boolean	allow_inverter_off
AllowInvOn	Boolean	allow_inverter_on
batt_abs_min	Real	batt_voltage_abs_min
batt_min_restart	Real	battery_voltage_min_restart
batt_min_start	Real	batt_voltage_min_start
batt_min_stop	Real	batt_voltage_min_stop
BattVolts	Real	battery_voltage
CmdManualMode	Boolean	ManualControlEnabled
CmdStartCompressor	Boolean	cmd_start_compressor
CmdStartInverter	Boolean	cmd_start_inverter
CmdStopCompressor	Boolean	cmd_stop_compressor
CmdStopInverter	Boolean	cmd_stop_inverter
CompressorStatus	Unsigned 16 bit integer	compressor_status
error_charger	Boolean	error_charger_modbus
error_inverter	Boolean	error_inverter_modbus
HeartBeat	Boolean	HeartBeat
InverterStatus	Boolean	inverter_status_running
min_restart_time	Real	min_restart_time
pv_abs_min	Real	pv_volts_min
pv_min_start	Real	pv_volts_min_start
PVVolts	Real	pv_voltage
show_buttons	Boolean	button_visible
time_day	Unsigned 16 bit integer	day
time_hr	Unsigned 16 bit integer	hour
time_min	Unsigned 16 bit integer	minute
time_month	Unsigned 16 bit integer	month

Table 23   Global Connection Tags

System Tag	Destination Tag
System Clock - Day	time_day
System Clock - Hour	time_hr
System Clock - Minute	time_min
System Clock - Month	time_month

C.   SCREENS

1.   Operation
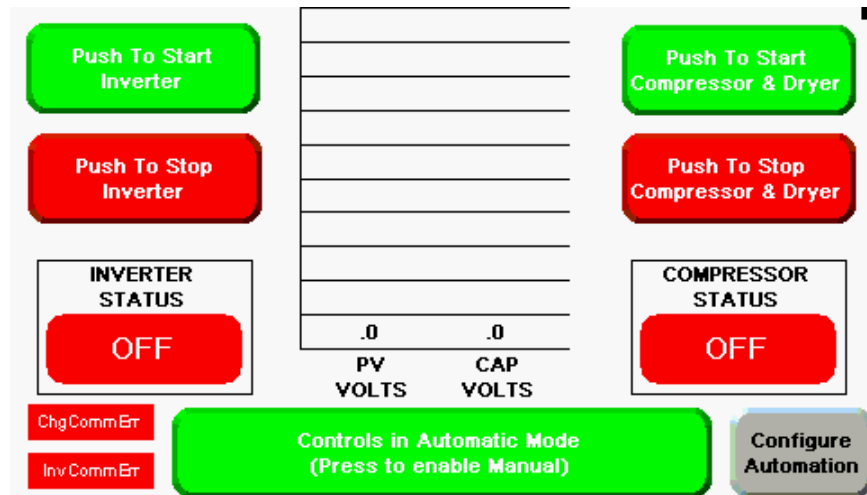
Figure 38.   HMI Operation Screen

Table 24   HMI Momentary Pushbutton Items

Item	Color	Caption Text	Write Tag
Push to Start Inverter			CmdStartInverter
State 0		Push to Start Inverter	
State 1		Starting Inverter	
		Error	
Push to Start Compressor & Dryer			CmdStartCompressor
State 0		Push to Start Compressor & Dryer	
State 1		Starting Compressor & Dryer	
		Error	
Push to Stop Inverter			CmdStopInverter
State 0		Push to Stop Inverter	
State 1		Stopping Inverter	
		Error	
Push to Stop Compressor & Dryer			CmdStopCompressor
State 0		Push to Stop Compressor & Dryer	
State 1		Stopping Compressor & Dryer	
		Error	

Table 25   HMI Multistate Indicator Items

Item	Color	Caption Text	Read Tag
Inverter Status			InverterStatus
State 0		OFF	
State 1		ON	
		ERROR	
Compressor Status			CompressorStatus
State 0		OFF	
State 1		RELAY ON	
State 2		RUNNING	
		ERROR	

Table 26   Maintained Pushbutton Items

Item	Color	Caption Text	Read & Write Tag
Control Mode			CmdManualMode
State 0	🟩	Controls in Automatic Mode (Press to enable Manual)	
State 1	🟥	Controls in Manual Mode (Press to Restore Automatic)	
	🟦	ERROR	

2. Settings

Figure 39.   HMI Settings Screen

Table 27   Numeric Increment Decrement Items

Label	Min Value	Max Value	Indicator & Write Tag
Abs Min Cap	0	51	batt_abs_min
Min Cap Run	0	53	batt_min_stop
Min Cap Start	0	53	batt_min_start
Min Cap Restart	0	53	batt_min_restart
Min Comp Off Time	0	60	min_restart_time
Min PV	0	70	pv_abs_min
Min PV Start	0	71	pv_min_start

Table 28   Numeric Display Items

Label	Read Tag
PV Array	PVVolts
Capacitor	BattVolts

APPENDIX E. MODBUS TESTING

This program is for the Allen-Bradley Micro850 to test Modbus communications. It allows the user to rapidly change the parameters of the Modbus message that is being sent, without having to compile and download the program to the controller repeatedly. Where a setting or variable property is not explicitly stated, it is in the default state.

A.   CONTROLLER PROGRAM

This section contains all of the information for the Micro850 controller Modbus testing program, AssignID.

1.   Controller Wide Settings

Table 29   Ethernet Settings

Setting	Value
Controller	
Ethernet	
Configure IP address and settings	Selected
IP Address:	192.168.0.1
Subnet Mask	255.255.255.0
Gateway Address	192.168.0.0

2. Global Variables

Table 30   Global Variables

Variable Name	Data Type	Initial Value
modbus_register	UDINT	
modbus_error	BOOL	FALSE
modbus_read	BOOL	FALSE
modbus_buffer	MODBUSLOCADDR	
modbus_run	USINT	0
modbus_cmd	USINT	4
modbus_data_cnt	UINT	1
modbus_read_data	UINT	0
modbus_buffer_loc	DINT	
modbus_write_data	UINT	0
modbus_write	USINT	0
modbus_unit_id	USINT	0
modbus_ip_ending	USINT	168

3. Function Block Diagram
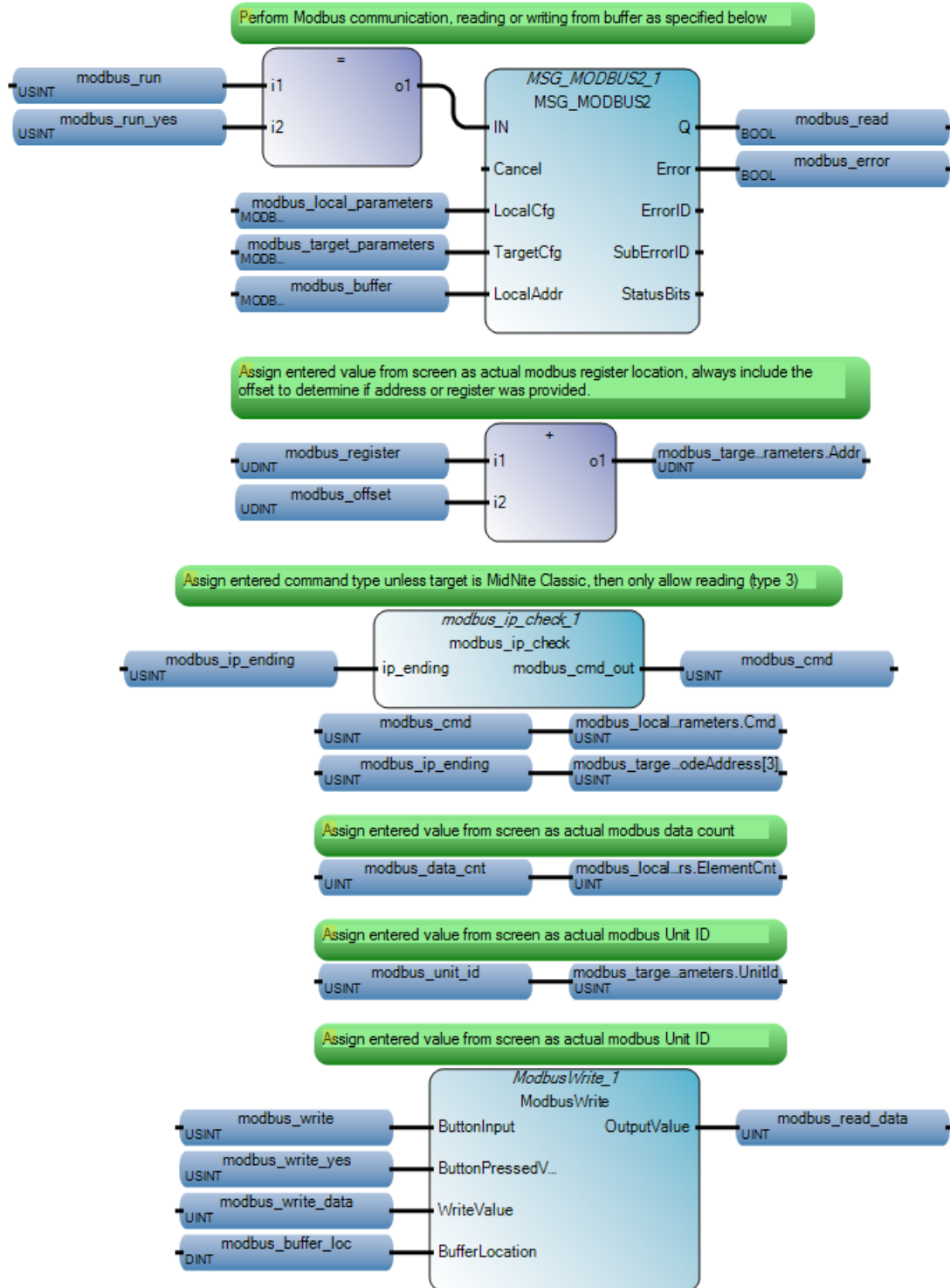

Figure 40.   AssignID Function Block Diagram

4. Local Variables

Table 31   AssignID Local Variables

Name	Data Type	Initial Value
modbus_local_parameters	MODBUS2LOCPARA	
Channel	UINT	4
TriggerType	UDINT	0
Cmd	USINT	3
ElementCnt	UINT	
modbus_target_parameters	MODBUS2TARPARA	
Addr	UDINT	
NodeAddress	MODBUS2NODEADDR	
NodeAddress[0]	USINT	192
NodeAddress[1]	USINT	168
NodeAddress[2]	USINT	0
NodeAddress[3]	USINT	168
Port	UINT	0
UnitId	USINT	
MsgTimeout	UDINT	0
ConnTimeout	UDINT	0
ConnClose	BOOL	TRUE
modbus_run_yes	USINT	1
modbus_write_yes	USINT	1
modbus_offset	UDINT	1

B.   USER-DEFINED FUNCTION BLOCKS

This section describes the user-defined function blocks used in the Modbus testing program AssignID.

1.   ModbusWrite:

This Structured Text style User-Defined Function Block will only write the specified data chunk (WORD) to the defined buffer location, provided all requirements are met. The buffer value then outputs for display.

a.   Structured Text

```
IF ButtonInput = ButtonPressedValue AND BufferLocation >
0 AND BufferLocation < 126 THEN
     modbus_buffer[BufferLocation] := WriteValue;
END_IF;

IF BufferLocation > 0 AND BufferLocation < 126 THEN
     OutputValue := modbus_buffer[BufferLocation];
ELSE
     OutputValue := 0;
END_IF;
```

b.   Local Variables

Table 32   ModbusWrite Local Variables

Name	DataType	Direction
ButtonInput	USINT	VarInput
ButtonPressedValue	USINT	VarInput
WriteValue	UINT	VarInput
BufferLocation	DINT	VarInput
OutputValue	UINT	VarOutput

2.   modbus_ip_check

This Structured Text style User-Defined Function Block only allows reading Modbus data if accessing the MidNite Classic charge controller. This is to prevent any problems due to accidentally overwriting important data on the controller, since the MidNite Classic will allow you to "write to any register in the system" [54].

a.   Structured Text

```
IF modbus_ip_ending = 50 THEN
     modbus_cmd_out := 3;
ELSE
     modbus_cmd_out := modbus_cmd;
END_IF;
```

b.   *Local Variables*

Table 33   modbus_ip_check Local Variables

Name	DataType	Direction
ip_ending	USINT	VarInput
modbus_cmd_out	USINT	VarOutput

C.   HMI PROGRAM

This section contains all of the information for the PanelView 800 HMI Modbus testing program. The HMI network was previously set up as indicated in Appendix B.

1.   HMI Settings

Table 34   Communication Settings

Name	Controller Type	Address
PLC-1	Micro800	192.168.0.1

2.   HMI Tags

Table 35   AssignUnitID Tags

Tag Name	Data Type	Address
modbus_address	Unsigned 32 bit integer	modbus_register
modbus_error	Boolean	modbus_error
modbus_cmd	Unsigned 8 bit integer	modbus_cmd
modbus_read_data	Unsigned 16 bit integer	modbus_read_data
modbus_buffer_loc	Unsigned 8 bit integer	modbus_buffer_loc
modbus_write_data	Unsigned 16 bit integer	modbus_write_data
modbus_run	Unsigned 8 bit integer	modbus_run
modbus_write	Unsigned 8 bit integer	modbus_write
modbus_unit_id	Unsigned 8 bit integer	modbus_unit_id
modbus_data_size	Unsigned 16 bit integer	modbus_data_cnt
modbus_ip_ending	Unsigned 8 bit integer	modbus_ip_ending

3. HMI Screens

Figure 41.   Main Screen

Table 36   Numeric Entry Items

Label	Min Value	Max Value	Indicator Tag	Write Tag
Register:	30001	65535		modbus_address
Type:	1	16	modbus_cmd	modbus_cmd
Unit ID:	1	247		modbus_unit_id
Data Size:	1	125		modbus_data_size
Item	1	125		modbus_buffer_loc
Value	0	65535		modbus_write_data
IP	0	255	modbus_ip_ending	modbus_ip_ending

Table 37   Momentary Push Button Items

Item	Color	Caption Text	Write Tag
Modbus Command			modbus_run
State 0		Modbus Commands Stopped	
State 1		Modbus Commands Sending	
		Error	
Modbus Buffer			modbus_write
State 0		Read Modbus Buffer	
State 1		Writing Modbus Buffer	
		Error	

83

Table 38   Numeric Display Items

| Label	Read Tag
Value	modbus_read_data

APPENDIX F. SUNNY WEBBOX UPDATE PROCEDURE

Use the same procedure to update either the firmware or the device profiles for the Sunny WebBox. This update procedure requires an SD card that is no larger than 2GB formatted with the FAT-16 file system. When performing multiple updates, the card does not need reformatting between updates. These instructions were adapted from [58].

A.   FORMATTING SD CARD AS FAT-16

- Insert the SD card into the computer's SD card reader.

- Open Windows Explorer and right click on the SD card to be formatted.

WARNING: ALL DATA ON THE SD CARD WILL BE LOST DURING FORMATTING. IF THE SD CARD CONTAINS IMPORTANT DATA, MAKE A BACKUP OF THE SD CARD FIRST.

- Click on "Format…"

- Set the File system to "FAT" and the Allocation unit size to "Default allocation size" as shown in Figure 42.

- Click Start.

- Read and acknowledge the warning dialog by pressing "OK."

- When the formatting process is complete, click "OK" to close the information window.

- Click "Close" to exit the formatting program.
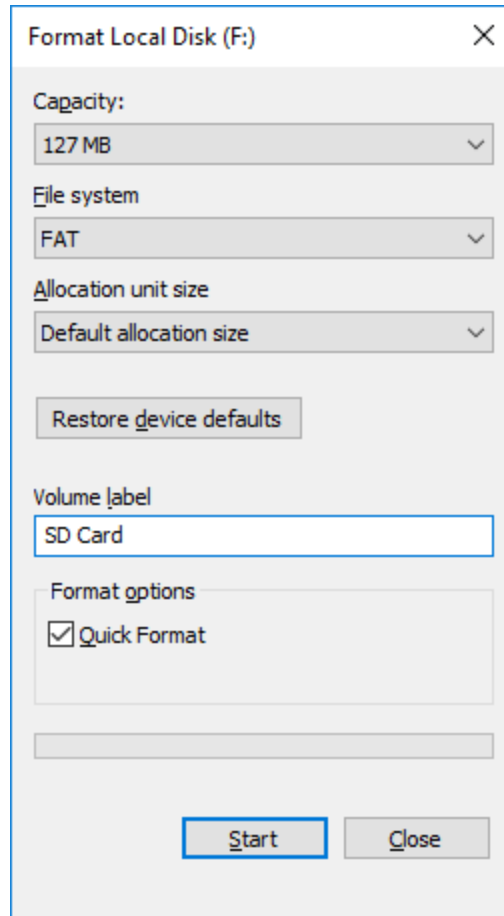
Shown with the appropriate selections made for formatting an SD card for use while updating WebBox firmware.

Figure 42.   Windows Format Utility

B.   FLASHING NEW FIRMWARE

Firmware update files for the WebBox are only available by contacting SMA directly via their customer support portal.

- Insert the SD card into the computer's SD card reader.

- Open Windows Explorer and navigate to the root directory of the SD card.

- Create a directory titled "Update" at the root of the SD card.

- Place the desired update file into the "Update" folder.

  Note: If the "Update" folder contains more than one file, the update will not occur.

86

- Remove the SD card from the computer's SD card slot.

- Insert the SD card into the WebBox SD card slot.

- Continue attempting to access the WebBox via the web interface at approximately 30-second intervals. The firmware update process is complete if the page loads.

THIS PAGE INTENTIONALLY LEFT BLANK

LIST OF REFERENCES

[1]   U.S. Energy Information Administration, 2017, "Monthly Energy Review," DOE/EIA-0035(2017/1), http://www.eia.gov/totalenergy/data/monthly/archive/00351701.pdf

[2]   American Geophysical Union, 2013, "Human-Induced Climate Change Requires Urgent Action," Washington, DC, https://sciencepolicy.agu.org/files/2013/07/AGU-Climate-Change-Position-Statement_August-2013.pdf

[3]   Pachauri, R. K., et al., 2014, "Climate Change 2014: Synthesis Report," IPCC, Geneva, Switzerland, doi:10.1515/igbp-2015-0001

[4]   U.S. Department of Energy, 2017, "Comprehensive Annual Energy Data and Sustainability Performance," http://ctsedwweb.ee.doe.gov/Annual/Report/HistoricalFederalEnergyConsumptionDataByAgencyAndEnergyTypeFY1975ToPresent.aspx

[5]   Smalley, D., 2012, "News: Energize: ONR Supports New Energy Partnership," Office of Naval Research, https://www.onr.navy.mil/en/Media-Center/Press-Releases/2012/Energy-Systems-Technology-ESTEP-ONR.aspx

[6]   Carlin, R., and Curtis, S., 2015, "ONR Program Evaluates Emerging Energy Technologies at Naval Facilities," Currents: The Navy's Energy & Environmental Magazine, **Fall 2015**, pp. 40-47.

[7]   Gardner, T, "U.S. military marches forward on green energy, despite Trump," 2017, http://www.reuters.com/article/us-usa-military-green-energy-insight-idUSKBN1683BL

[8]   Beitman, A, 2017, "Report: Clean Energy Jobs Overwhelm Coal, Oil & Gas in 41 States and D.C.," http://content.sierraclub.org/press-releases/2017/03/attention-donald-trump-new-report-shows-clean-energy-employs-far-more-workers

[9]   Cuff, M, 2016, "5 things to know about the $329 billion clean energy boom," https://www.greenbiz.com/article/5-things-know-about-329-billion-clean-energy-boom

[10]   Frankfurt School of Finance & Management gGmbH, 2017, "Global Trends in Renewable Energy Investment 2017," 2017, http://fs-unep-centre.org/sites/default/files/publications/globaltrendsinrenewableenergyinvestment2017.pdf.

[11]   Lazard LTD., 2016, "Levelized Cost of Energy Analysis 10.0," https://www.lazard.com/media/438038/levelized-cost-of-energy-v100.pdf

[12]   Kondoh, J, et al., 2000, "Electrical Energy Storage Systems for Energy Networks," Energy Conversion and Management, **41**(17), pp. 1863-1874.

[13]   Werber, C, 2017, "California is getting so much power from solar that electricity prices are turning negative," https://qz.com/953614/california-produced-so-much-power-from-solar-energy-this-spring-that-wholesale-electricity-prices-turned-negative/

[14]   Vaughan, A., 2017, "UK households spent £180m on 'unnecessary' power capacity – report," https://www.theguardian.com/business/2017/mar/13/uk-households-unnecessary-power-capacity-energy-climate-intelligence-unit-report

[15]   Foley, A. M., et al., 2012, "Current methods and advances in forecasting of wind power generation," Renewable Energy, **37**(1), pp. 1-8.

[16]   U.S. Department of Energy, 2013, "Grid Energy Storage," Washington, DC, https://energy.gov/sites/prod/files/2014/09/f18/Grid%20Energy%20Storage%20December%202013.pdf

[17]   Lazard LTD., 2016, "Levelized Cost of Storage Analysis 2.0," www.lazard.com/media/438042/lazard-levelized-cost-of-storage-v20.pdf.

[18]   Vranas, T, 2017, "Control System Development for Power Generation From Small-Scale Compressed Air Energy Storage," M.S. thesis, Dept. of Mech. Eng., Naval Postgraduate School, Monterey, CA.

[19]   Denholm, P., et al., 2010, "Role of Energy Storage with Renewable Electricity Generation," NREL/TP-6A2-47187, http://www.osti.gov/scitech/biblio/972169

[20]   Luo, X., et al., 2015, "Overview of current development in electrical energy storage technologies and the application potential in power system operation," Applied Energy, **137**, pp. 511-536

[21]   Sullivan, P., Short, W., and Blair, N., 2008, "Modeling the Benefits of Storage Technologies to Wind Power," Wind Engineering, **32**(6), pp. 603-615.

[22]   van der Linden, S., 2007, "Integrating Wind Turbine Generators (WTG's) With GT-CAES (Compressed Air Energy Storage) Stabilizes Power Delivery With the Inherent Benefits of Bulk Energy Storage," IMECE2007-41853, *ASME 2007 International Mechanical Engineering Congress and Exposition*, **6**, pp. 379-386.

[23]   Dunn, B., Kamath, H., and Tarascon, J.-M., 2011, "Electrical Energy Storage for the Grid: A Battery of Choices," Science, **334**(6058), pp. 928-935.

[24]   Arnulfi, G. L., and Marini, M., 2006, "Management Strategies for a Compressed Air Energy Storage Plant," GT2006-90437, *ASME Turbo Expo 2006: Power for Land, Sea and Air*, **4**, pp. 133-142.

[25]   Ter-Gazarian, A. G., 2011, *Energy Storage for Power Systems (2nd Edition)*, The
        Institution of Engineering and Technology, London, United Kingdom, Chap. 7.

[26]   Junkermann, W., Vogel, B., and Sutton, M. A., 2011, "The climate penalty for
        clean fossil fuel combustion," Atmospheric Chemistry and Physics, **11**(24), pp.
        12917-12924.

[27]   Kurz, R., 2005, "Gas Turbine Performance," *Proceedings of the Thirty-Fourth
        Turbomachinery Symposium*, Texas A&M University System, Houston, Texas,
        pp. 131-146.

[28]   van der Linden, S., 2006, "Bulk energy storage potential in the USA, current
        developments and future prospects," Energy, **31**(15), pp. 3446-3457.

[29]   Funk, J., 2013, "FirstEnergy postpones project to generate elecricity with
        compressed air," http://www.cleveland.com/business/index.ssf/2013/07/
        firstenergy_postpones_project.html

[30]   Haugen, D., 2012, "Scrapped Iowa project leaves energy storage lessons,"
        http://midwestenergynews.com/2012/01/19/scrapped-iowa-project-leaves-energy-
        storage-lessons/

[31]   Bullough, C., et al., 2004, "Advanced Adiabatic Compressed Air Energy Storage
        for the Integration of Wind Energy," APL000053, *Proceedings of the European
        Wind Energy Conference*, pp. 1-8.

[32]   Moran, M. J., and Shapiro, H. N., 2008, *Fundamentals of Engineering
        Thermodynamics*, John Wiley & Sons Inc., Hoboken, NJ, Chap. 6.

[33]   Jakiel, C., Zunft, S., and Nowi, A., 2007, "Adiabatic compressed air energy
        storage plants for efficient peak load power supply from wind energy: the
        European project AA-CAES," International Journal of Energy Technology and
        Policy, **5**(3), pp. 296-306.

[34]   Energiespeicher Forschungsinitiative der Bundesregierung, 2016, "Druckluft-
        statt Pumpspeicher," http://forschung-energiespeicher.info/projektschau/
        gesamtliste/projekt-einzelansicht/95/Druckluft_statt_Pumpspeicher/

[35]   RWE Power AG, 2010, "ADELE - Adiabatic Compressed-Air Energy Storage for
        Electricity Supply," Spohr's Büro für Kommunikation GmbH, Cologne,
        Germany.

[36]   Barbour, E., et al., 2015, "Adiabatic Compressed Air Energy Storage with packed
        bed thermal energy storage," Applied Energy, **155**, pp. 804-815.

[37]   Petrov, M. P., Arghandeh, R., and Broadwater, R., 2013, "Concept and Application of Distributed Compressed Air Energy Storage Systems Integrated in Utility Networks," POWER2013-98113, *Proceedings of the ASME Power Conference*, **2**, pp. 1-8.

[38]   Jannelli, E., et al., 2014, "A small-scale CAES (compressed air energy storage) system for stand-alone renewable energy power plant for a radio base station: A sizing-design methodology," Energy, **78**, pp. 313-322.

[39]   Patel, S. M., Freeman, P. T., and Wagner, J. R., 2014, "An Electrical Microgrid: Integration of Solar Panels, Compressed Air Storage, and a Micro-Cap Gas Turbine," DSCC2014-6058, *Proceedings of the ASME 2014 Dynamic Systems and Control Conference*, **2**, pp. 1-10.

[40]   Hawxhurst, K. L. J., 2016, "Microgrid Control Strategy Utlizing Thermal Energy Storage With Renewable Solar and Wind Power Generation," M.S. thesis, Dept. of Mech. Eng., Naval Postgraduate School, Monterey, CA.

[41]   McLaughlin, C. S., 2016, "Small-Scale Air-Driven Generator," M.S. thesis, Dept. of Mech. Eng., Naval Postgraduate School, Monterey, CA.

[42]   Prinsen, T. H., 2016, "Design and Analysis of a Solar-Powered Compressed Air Energy Storage System," M.S. thesis, Dept. of Mech. Eng., Naval Postgraduate School, Monterey, CA.

[43]   Solarworld AG, 2017, "Sunmodule Plus," http://www.solarworld.de/fileadmin/ downloads_new/produkt/sunmodule/datenblaetter/en/mono/sw_sunmodule_plus_ 280-290_monoblack_5bb_en.pdf

[44]   Salas, V., et al., 2006, "Review of the maximum power point tracking algorithms for stand-alone photovoltaic systems," Solar Energy Materials and Solar Cells, **90**(11), pp. 1555-1578.

[45]   Home Power Inc., 2017, "Maximum Power Point Tracking (MPPT)," https://www.homepower.com/maximum-power-point-tracking-mppt

[46]   Nave, C. R., 2017, "Energy Stored on a Capacitor," http://hyperphysics.phy-astr.gsu.edu/hbase/electric/capeng2.html

[47]   Maxwell Technologies Inc., 2013, "Datasheet | 56V Module," http://www.maxwell.com/images/documents/56vmodule_ds_1017119-3.pdf

[48]   Daggett, R., 2013, "PC-Based Controls vs. PLC-Based Controls for Machine Automation," https://www.bastiansolutions.com/blog/index.php/2013/04/24/pc-based-controls-vs-plc-based-controls-for-machine-automation/

[49] Mahaffey, T.R., 2002, "Electromechanical Relays Versus Solid-State: Each Has Its Place," http://electronicdesign.com/components/electromechanical-relays-versus-solid-state-each-has-its-place

[50] SMA America LLC, 2012, "Off-grid Inverter Sunny Island 4548-US/6048-US Technical Description," http://www.midnitesolar.com/pdfs/SI45_60-eng-TB-TUS120812.pdf

[51] Brooks, P., 2001, "EtherNet/IP: Industrial Protocol White Paper," Institute of Electrical and Electronic Engineers, http://literature.rockwellautomation.com/idc/groups/literature/documents/wp/enet-wp001_-en-p.pdf

[52] Siemens Corporation, 2007, "History of the Modbus protocol," http://w3.usa.siemens.com/us/internet-dms/btlv/CircuitProtection/Molded CaseBreakers/docs_MoldedCaseBreakers/Modbus%20Information.doc

[53] SMA America L.L.C., 2014, "SUNNY WEBBOX Modbus® Interface," http://files.sma.de/dl/2585/WEBBOX-MODBUS-TB-en-19.pdf

[54] MidNite Solar Inc., 2013, "MidNite Solar MODBUS Network Spec," http://www.midnitesolar.com/pdfs/classic_register_map_Rev-C5-December-8-2013.pdf

[55] Saidur, R., et al., 2012, "Applications of variable speed drive (VSD) in electrical motors energy savings," Renewable and Sustainable Energy Reviews, **16**(1), pp. 543-550.

[56] Rockwell Automation Inc., 2015, "Connected Components Workbench 9.0 Help."

[57] The United States Naval Observatory, 2016, "Sun or Moon Rise/Set Table for One Year," http://aa.usno.navy.mil/data/docs/RS_OneYear.php

[58] SMA America L.L.C., 2013, "SUNNY WEBBOX," http://files.sma.de/dl/4253/SWebBox-BA-US-en-34.pdf

THIS PAGE INTENTIONALLY LEFT BLANK

INITIAL DISTRIBUTION LIST

1.   Defense Technical Information Center
        Ft. Belvoir, Virginia

2.   Dudley Knox Library
        Naval Postgraduate School
        Monterey, California